

A High-Speed Time-Optimal Trajectory Generation Strategy via a Two-layer Planning Model[★]

Haotian Tan, Yuan-Hua Ni

College of Artificial Intelligence, Nankai University, Tianjin 300350, PR China

Abstract

MPC (Model predictive control)-based motion planning and trajectory generation are essential in applications such as unmanned aerial vehicles, robotic manipulators, and rocket control. However, the real-time implementation of such optimization-based planning faces significant challenges arising from non-convex problem structures and inherent limitations of nonlinear programming—notably the difficulty in guaranteeing solution quality and the unpredictability of computation time. To improve robustness and computational efficiency, this paper introduces a two-layer motion planning algorithm for intelligent ground vehicles based on convex optimization. The proposed algorithm iteratively constructs discrete optimal control subproblems with small, fixed terminal times, referred to as planning cycles. Each planning cycle is further solved within progressively constructed convex sets generated by utilizing customized search algorithms. The entire solution to the original problem is obtained by incrementally composing the solutions of these subproblems. The proposed algorithm demonstrates enhanced reliability and significantly reduced computation time. We support our approach with theoretical analysis under practical assumptions and numerical experiments. Comparative results with standard sequential convex programming (SCP) methods demonstrate the superiority of our method—include a significant improved computational speed under dynamic environments while maintain a near optimal final time.

Key words: Trajectory optimization; convex programming; artificial potential field

1 Introduction

As industrial technology continues to advance, a growing number of automotive devices have been developed, making trajectory generation a crucial area of research. Trajectory generation and motion planning focus on determining appropriate control strategies for agents—such as robots, drones, and other autonomous systems—to navigate from a starting point to a target while avoiding obstacles. An efficient planning algorithm is essential, as it can significantly reduce energy consumption and travel time while ensuring safety, ultimately leading to considerable economic benefits. Over the past decades, numerous planning algorithms have been developed. Despite varying methodologies and application contexts, these approaches can be broadly classified into three main categories [1]: search-based, sampling-based, and optimization-based methods. Among search-based algorithms, the A* algorithm, introduced in 1968 [2], efficiently identifies optimal paths using heuristic func-

tions [3]. However, it faces high computational demands in large-scale or dense grid environments [4]. Subsequent enhancements such as D* [5], which supports dynamic replanning in response to new obstacles, and ARA* [6], which improves efficiency through incremental search, have improved the adaptability. Nevertheless, these variants still inherit the core scalability limitations of A*, restricting their use in large-scale real-time applications.

In the domain of sampling-based algorithms, the Rapidly-exploring Random Tree (RRT) method offers an effective framework for obstacle avoidance by probabilistically exploring the configuration space [7]. While standard RRT is valued for its simplicity and flexibility, its variant RRT* [8] achieves asymptotic optimality at the expense of higher computational load. Although many RRT extensions have shown advantages in specific applications [9], issues such as hardware limitations and kinematic infeasibility continue to restrict their broader adoption. **Complementary to sampling-based approaches, the advancement of model predictive control (MPC) has enabled systematic solution of trajectory generation problems through optimization techniques.** Indirect methods, such as those employing Pontryagin's maximum principle or Lagrange multipliers

[★] This work is supported in part by the National Natural Science Foundation of China (62173191)

Email addresses: ElmundoTan@outlook.com (Haotian Tan), yhni@nankai.edu.cn (Yuan-Hua Ni).

[10] [11], offer analytical insights but are often computationally challenging due to sensitivity to initial conditions and implementation complexity. In contrast, direct methods reformulate the optimal control problem into nonlinear programming (NLP) via parameterization and discretization, allowing numerical solutions using Newton’s method [12], ADMM [13], [14] or heuristic (e.g., genetic algorithms) approaches. The common parameterization and discretization methods include direct shooting method, collocation method and Pseudo-Spectrum Method, etc. Discrete optimization problems of this type are generally NP-hard and thus unsuitable for real-time onboard computation. Fortunately, convexification techniques can yield tractable solutions for specific problem classes by exploiting the efficiency of convex optimization. For non-convex input constraints—such as minimum thrust in rocket models—lossless convex relaxation [expands](#) the control vector to transform constraints into convex forms [15]. Despite introducing additional variables, the relaxed problem remains easier to solve due to its convex structure. For non-convex state constraints like obstacle avoidance, sequential convex programming can rapidly produce feasible trajectories [16], though it may converge to suboptimal solutions [17]. Techniques such as adding trust regions [18], tightening approximations, or softening constraints can mitigate ill-conditioning and reduce artificial infeasibility [19]. Direct optimization methods are widely used in time-optimal control. As for discrete model predictive control problems are relatively straightforward to formulate, line search methods can be effectively employed to determine the optimal control time. Alternatively, time-optimal control can also be addressed by solving a series of fixed-time optimal control subproblems iteratively [20]. However, this method depends heavily on extensive map information and typically lacks terminal constraints, which may restrict its practical applicability.

This paper addresses the problem of generating collision-free trajectories in environments with static and dynamic obstacles. To enhance solution quality and time optimality in motion planning, we propose a dynamic trajectory generation algorithm based on an iterative two-layer optimization framework. Each iteration employs a small [period](#) planning cycle with fixed final time, which is decomposed into two trajectory optimization subproblems and a trajectory search step. By incrementally construct planning cycles and concatenate segmented control inputs, the method produces a globally admissible control sequence capable of dynamic obstacle avoidance. Furthermore, we introduce two trajectory search algorithms for the optimization loop and analyze their feasibility conditions. The main contributions of this work are summarized as follows.

- We employ trajectory searching methods to generate restricted convex regions guided by nominal solutions, effectively mitigating non-convexity while maintaining feasibility. Additionally, we propose a customized

artificial potential field method with kinematic reliability to serve as the trajectory search algorithm. This tailored approach can also function independently as a standalone planning algorithm in specific case.

- Our proposed algorithms have been validated to generate trajectories that achieve an approximately [local optimal control time](#) under specified conditions and moderate assumptions. Compared with conventional motion planning solvers based on sequential convex programming, the proposed method exhibits enhanced robustness in dynamic environments while substantially reducing computational overhead—findings supported by numerical experiments, which demonstrate both a higher success rate and shorter total computation time.
- By decomposing the complete problem into planning cycles and solving one planning cycle in parallel mode while moving, we have developed a robust framework that ensures both reliability and precision while only relying on a part of map information at a specific time.

In the remainder of this paper, Section II formulates the optimal control problem and establishes the theoretical foundation for our approach. Section III introduces the two-layer optimization model and develops the corresponding trajectory search algorithms, along with a thorough analysis of their properties and effectiveness. Section IV presents numerical experiments conducted in both static and dynamic environments. Finally, Section V concludes the paper with a summary of findings.

Notations: throughout the subsequent sections, all sets are defined in \mathbb{R}^n with context-specific n , and the [Euclidean norm](#) $\|\mathbf{a}\| = \sqrt{\langle \mathbf{a}, \mathbf{a} \rangle} = \sqrt{\mathbf{a}^\top \mathbf{a}}$, and we further let $\|\mathbf{a}\|_Q = \sqrt{\mathbf{a}^\top Q \mathbf{a}}$ with [Q being a positive definite weighting matrix](#). The diameter of a set $\mathcal{S} \subset \mathbb{R}^n$ is defined as

$$\text{diam}(\mathcal{S}) := \begin{cases} 0, & \mathcal{S} = \emptyset, \\ \sup\{\|\mathbf{y} - \mathbf{x}\| : \mathbf{x}, \mathbf{y} \in \mathcal{S}\}, & \text{else,} \end{cases}$$

and for some $\mathbf{x}_0 \in \mathbb{R}^n$ with non-negative real number d , we denote by $\mathcal{B}(\mathbf{x}_0, d)$ the closed ball centered at \mathbf{x}_0 with radius d :

$$\mathcal{B}(\mathbf{x}_0, d) := \{\mathbf{x} \in \mathbb{R}^n : \|\mathbf{x} - \mathbf{x}_0\| \leq d\}.$$

Sliced vectors are denoted $\mathbf{a}[i : j]$, representing rows i to j of column vector \mathbf{a} (e.g., $\mathbf{a} = [a_1, a_2, a_3, a_4]^\top \Rightarrow \mathbf{a}[2 : 3] = [a_2, a_3]^\top$). For a set $\mathcal{S} \subseteq \mathbb{R}^{\ell_s}$, the sliced set is defined as

$$\mathcal{S}[a : b] := \{\mathbf{x}[a : b] \mid \mathbf{x} \in \mathcal{S}\}.$$

The gradient of a differentiable function $f : \mathbb{R}^n \mapsto \mathbb{R}$ is denoted $\nabla f(\mathbf{x}) := \left[\frac{\partial f}{\partial x_1}, \dots, \frac{\partial f}{\partial x_n} \right]^\top$. We use $\text{Null}(\cdot)$ for the null space, and $\text{cl}(\cdot)$, $\text{conv}(\cdot)$ for the closure and convex hull respectively. The term *speed* refers to the Euclidean norm of velocity.

2 Problem Formulation

2.1 Classic Framework

Trajectory generation aims to compute feasible and safe trajectories for a vehicle within a structured environment \mathcal{M} —referred to as the map—that contains obstacles, a target region, and an initial state. In this paper, \mathcal{M} is defined in a unified Euclidean space. Each obstacle is denoted as \mathcal{O}_i for $i \in \{1, 2, \dots, n_{obs}\}$, with n_{obs} the total number of obstacles. The volume occupied by the vehicle is represented by \mathcal{V} . As \mathcal{M} is generally bounded, we assume that each \mathcal{O}_i is bounded and that $\mathcal{V} \subset \mathcal{M}$ holds at all times. This simplification allows us to focus on the core contributions without loss of generality, as the map containment constraints can be incorporated when needed. Collisions are strictly prohibited throughout the task, expressed mathematically as:

$$\mathcal{O}_i \cap \mathcal{V} = \emptyset, \quad i \in \{1, 2, \dots, n_{obs}\}. \quad (1)$$

For irregularly shaped obstacle regions \mathcal{O}_i , obtaining exact analytic descriptions is often intractable. To overcome this challenge, we adopt an approximation involves enclosing each obstacle region \mathcal{O}_i within a union of closed balls. Specifically, there must exist some positions $x, p_1, p_2, \dots, p_{n_{obs}} \in \mathcal{M}$ with

$$\mathcal{O}_i \subseteq \mathcal{B}(p_i, \text{diam}(\mathcal{O}_i)/2) \quad (2)$$

for $i = 1, 2, \dots, n_{obs}$, and

$$\mathcal{V} \subseteq \mathcal{B}(x, \text{diam}(\mathcal{V})/2). \quad (3)$$

For conciseness, we denote $\mathcal{B}_i := \mathcal{B}(p_i, \text{diam}(\mathcal{O}_i)/2)$ and $\mathcal{B}_{\mathcal{V}} := \mathcal{B}(x, \text{diam}(\mathcal{V})/2)$ for such $x, p_1, \dots, p_{n_{obs}}$. Thus, an approximated scenario can be created by substitute $\mathcal{O}_i, \mathcal{V}$ with $\mathcal{B}_i, \mathcal{B}_{\mathcal{V}}$. In the approximated scenario, prior knowledge of obstacle shapes is no longer required, significantly simplifying the design of subsequent algorithms. Consequently, the obstacle avoidance constraints can be expressed as

$$\|x - p_i\| \geq \frac{\text{diam}(\mathcal{O}_i) + \text{diam}(\mathcal{V})}{2} := r_i, \quad (4)$$

where x, p_i and $r_i \geq 0$ are critical parameters used in constructing the planning problem. This shape approximation relies on two key assumptions, formalized as Assumptions 1 and 2 below.

Assumption 1 Given the map, both the initial and target positions lie outside all obstacle regions \mathcal{B}_i for $i \in \{1, 2, \dots, n_{obs}\}$.

Assumption 2 For any pair of indices $i, j \in \{1, \dots, n_{obs}\}$ with $i \neq j$, the obstacle regions are mutually disjoint. Furthermore, we assume the existence of a positive constant ℓ that

$$\mathcal{B}(p_i, r_i + 0.5\ell) \cap \mathcal{B}(p_j, r_j + 0.5\ell) = \emptyset$$

for all $i \neq j$.

Assumption 1 serves as the foundational premise underpinning all subsequent analyses. Assumption 2 introduces a more flexible condition, which can be intuitively understood as allowing multiple small obstacles—along with the gaps between them—to be treated as a single larger obstacle, as illustrated in Fig. 1. It is therefore evident that Assumption 2 is relatively mild.

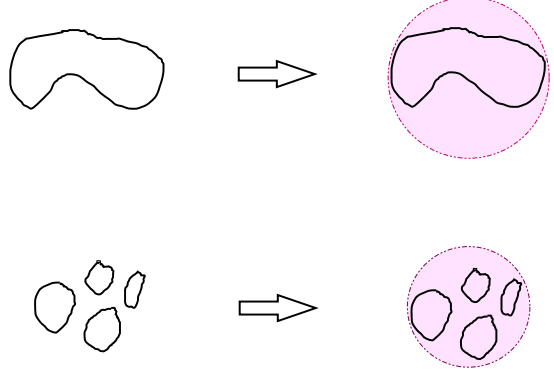


Fig. 1. A single irregular obstacle (top left) can be approximated by a closed ball (top right), while multiple densely clustered small obstacles (bottom left) may be merged into a larger enclosing ball (pink circle, bottom right) for simplified representation.

In this work, we define the state vector as $z(t) := [x^\top, \dot{x}^\top]^\top$ and consider a control-affine dynamic system

$$\dot{z}(t) = f_c(z, u) = f_a(z) + f_b(z) \cdot u, \quad (5)$$

where f_c is differentiable and u denotes the control input. Physical constraints are given by $z^\top Q_1 z \leq 1$ and $u^\top Q_2 u \leq 1$, with Q_1, Q_2 being strictly positive definite weighting matrices. These constraints reflect practical limitations such as maximum speed limits ($\|\dot{x}\| \leq v_{\max}$), control input bounds ($\|u\| \leq u_{\max}$), and friction effects. Let z_0 and z_f as the initial and one of the target state, respectively. The boundary constraints are then expressed as

$$z(0) = z_0, \quad (6)$$

$$\|z(t_f) - z_f\|_{Q_0} \leq \gamma, \quad (7)$$

where Q_0 is a positive definite weighting matrix, t_f denotes the final time profiling the task's time cost, $z(t_f)$ is the ending state and (7) profiles the target area.

With the objective of minimizing the control time, the original trajectory optimization problem is formulated as

$$\min_{z, u} \quad t_f \quad (8)$$

$$\text{s.t. } (5) - (7), \quad (9)$$

$$\|z\|_{Q_1}^2 \leq 1, \quad \|u\|_{Q_2}^2 \leq 1. \quad (10)$$

To enable numerical optimization, the continuous problem must be discretized and parameterized. Given a fixed time step h , substitute $z(t)$ by $\{z_1, \dots, z_{N+1}\}$ and $u(t)$ by $\{u_1, \dots, u_N\}$ with h as the sampling period, (5) can be then discretized into the algebraic form:

$$\begin{aligned} z_{i+1} - z_i &= h f_c(z_i, u_i), \\ \Rightarrow z_{i+1} &:= f(z_i, u_i). \end{aligned} \quad (11)$$

We denote $\{z_1, \dots, z_{N+1}; u_1, \dots, u_N\}$ by $\{Z; U\}_N$, then a discretized optimization problem \mathcal{P}_0 is obtained as

$$\begin{aligned} \min_{\{Z; U\}_N} \quad & Nh \\ \text{s.t.} \quad & (11), \\ & G_1(z_i) := z_i^\top Q_1 z_i - 1 \leq 0, \quad (12) \\ & G_2(u_i) := u_i^\top Q_2 u_i - 1 \leq 0, \quad (13) \\ & z_1 = z_0, \quad (14) \\ & \|z_{N+1} - z_f\|_{Q_0} \leq \gamma, \quad (15) \\ & \|z_i[1:2] - p_j\| \geq r_j, 1 \leq j \leq n_{obs}. \quad (16) \end{aligned}$$

2.2 Our Proposed Framework

We assume \mathcal{P}_0 is solvable. As \mathcal{P}_0 exhibits a typical structure commonly found in related literature, this assumption is mild, and also necessary. However, solving \mathcal{P}_0 quickly and robustly remains challenging due to its non-convex nature. In our framework, \mathcal{P}_0 is not solved directly. Instead, we iteratively construct and solve discretized approximated problems using a fixed time step h and pre-selected N . By concatenating the resulting trajectory segments, \mathcal{P}_0 can be effectively solved under mild assumptions.

We further linearize (11) as

$$z_{i+1} := A(z_0)z_i + B(z_0)u_i + w(z_0), \quad (17)$$

where $A_c(z_0), B_c(z_0)$ are the Jacobi matrices of f at z_0 , and $w_c(z_0)$ denotes the draft. In the most special case, if $u(t)$ represents the acceleration, then we have

$$A_c(\cdot) \equiv \begin{pmatrix} \mathbf{0}_{2 \times 2} & \mathbf{I}_{2 \times 2} \\ \mathbf{0}_{2 \times 2} & \mathbf{0}_{2 \times 2} \end{pmatrix}, B_c(\cdot) \equiv \begin{pmatrix} \mathbf{0}_{2 \times 2} \\ \mathbf{I}_{2 \times 2} \end{pmatrix}, w_c(\cdot) \equiv 0,$$

where $\mathbf{I}_{2 \times 2}$ is the 2-dimensional identity matrix, $\mathbf{0}_{2 \times 2}$ is the 2×2 zero matrix. Let

$$J(z_i, u_i) = [z_f - z_{N+1}]^\top Q_0 [z_f - z_{N+1}], \quad (18)$$

then two problems classes can be formulated as $\mathcal{P}_1(z_0; N)$:

$$\begin{aligned} \min_{\{Z; U\}_N} \quad & (18) \\ \text{s.t.} \quad & (11), (12) - (14), (16) \end{aligned}$$

and $\mathcal{P}'_1(z_0; N; A(z_0), B(z_0))$:

$$\min_{\{Z; U\}_N} \quad (18)$$

$$\text{s.t.} \quad (12) - (14), (16), (17)$$

In the subsequent content, when no ambiguity arises, we also adopt the simplified notations $\mathcal{P}_1(\cdot), \mathcal{P}_1(z_0; \cdot), \mathcal{P}'_1(\cdot), \mathcal{P}'_1(z_0; \cdot)$, etc. In both problem classes, N is referred to as the horizon, Nh is called the **control time**. Throughout our method, \mathcal{P}_0 is solved equivalently by solving some $\mathcal{P}_1(\cdot)$ with small Nh iteratively. For weakly nonlinear systems with sufficiently short control times, the use of approximated dynamics—with continuous updates to $A(z_0), B(z_0)$, and $w(\cdot)$ —preserves solution accuracy. That is, the solution of $\mathcal{P}'_1(z_0; N; A(z_0), B(z_0))$ closely approximates that of $\mathcal{P}_1(z_0; N)$. Therefore, the short-control time problem $\mathcal{P}_1(\cdot)$ can be replaced by $\mathcal{P}'_1(z_0; N; A(z_0), B(z_0))$, while $z_0, N, A(z_0)$, and $B(z_0)$ are updated in real time to maintain precision. The formulating and solving of $\mathcal{P}_1(z_0; N)$ is called a **planning cycle**.

3 Algorithm and Analysis

As the solution of \mathcal{P}_0 is obtained by iteratively run planning cycles, each planning cycle is further computed through three sequential subroutines in our works. At the start of each planning cycle, the current state z_0 along with matrices $A(z_0)$ and $B(z_0)$ are determined to formulate $\mathcal{P}'_1(\cdot)$. Then, a relaxed version of $\mathcal{P}'_1(\cdot)$ —called the relaxed problem—is solved to generate a nominal solution and extract a collision-free convex region, and a strict convex optimization within this region is formulated to compute the final trajectory segment. This convex-styled process maintains the robustness and fasten the computation. This section provides a detailed breakdown of these steps and conducts the corresponding mathematical analyses to validate their efficacy.

3.1 Reformulation of Planning Cycles

With given $z_0, N, A(z_0), B(z_0)$, we denote the relaxed problem by $\mathcal{P}_r(z_0; N; A(z_0), B(z_0))$, which derived from $\mathcal{P}'_1(z_0; N; A(z_0), B(z_0))$ while (15) and all the non-convex obstacle avoiding constraints (16) are removed, i.e. we have $\mathcal{P}_r(z_0; N, A(z_0), B(z_0))$:

$$\begin{aligned} \min_{\{Z; U\}_N} \quad & (18) \\ \text{s.t.} \quad & (12) - (14), (17). \end{aligned}$$

The convexity of $\mathcal{P}_r(\cdot)$ is ensured since (15) is not considered in this problem. If $\mathcal{P}_r(z_0; N; A(z_0), B(z_0))$ is solvable, then its optimizer is referred to as the nominal solution of $\mathcal{P}_r(z_0; N; A(z_0), B(z_0))$.

Remark 1 Note that we have $z_1 = z_0$ according to (14). Therefore, $\mathcal{P}_1(z_0; N)$ and $\mathcal{P}'_1(z_0; N; \cdot)$ can also be seen as optimization problems of $\{z_2, \dots, z_{N+1}, u_1, \dots, u_N\}$.

Suppose is a constraint-complaint solution of $\mathcal{P}'_1(z_0; N; A(z_0), B(z_0))$ denoted by

$$F := \{\tilde{z}_1, \dots, \tilde{z}_{N+1}; \tilde{u}_1, \dots, \tilde{u}_N\},$$

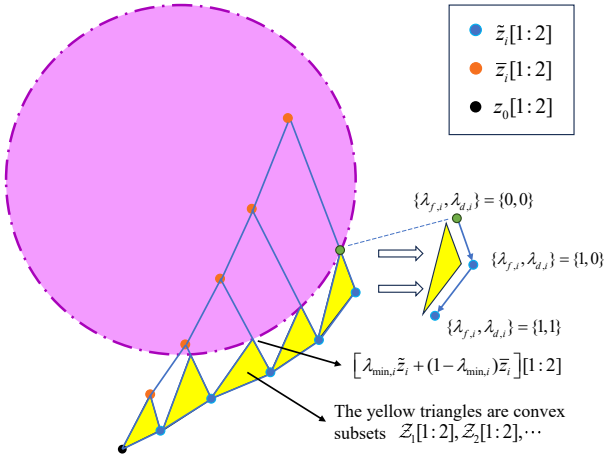


Fig. 2. A Visualization of obtaining Z_i

$\{\bar{z}_1, \dots, \bar{z}_{N+1}; \bar{u}_1, \dots, \bar{u}_N\}$ is the optimizer of the corresponding $\mathcal{P}_r(z_0; N; A(z_0), B(z_0))$, then a linear interpolation can be implemented as

$$z_i[1 : 2] = (\lambda \bar{z}_i + (1 - \lambda) \bar{z}_i)[1 : 2],$$

where a given λ determines the unique $z[1 : 2]$. The method for obtaining F is referred to as the **searching algorithm**, which will be detailed in a later subsection. Building upon the interpolation method, as $\bar{z}_i[1 : 2]$ is collision-free points, we define $\lambda_{\min} := \{\lambda_{\min,1}, \lambda_{\min,2}, \dots, \lambda_{\min,N+1}\}$ with

$$\lambda_{\min,i} = \max \left(\bigcup_{j=1}^{n_{\text{obs}}} \left\{ \max \left\{ \lambda_i : \exists p_j, r_j, \|z_i[1 : 2] - p_j\| = r_j \right\}, 0 \right\} \right).$$

Under the definition of $\lambda_{\min,i}$, any $z_i[1 : 2] = (\lambda \bar{z}_i + (1 - \lambda) \bar{z}_i)[1 : 2]$ with $0 < \lambda_{\min,i} < \lambda < 1$ is a collision-free point in \mathcal{M} , while $[\lambda_{\min,i} \bar{z}_i + (1 - \lambda_{\min,i}) \bar{z}_i][1 : 2]$ lies on the edge of one obstacle if $\lambda_{\min,i} = 0$. By further introducing variables $\lambda_{f,i}$ and $\lambda_{d,i}$ with $i = 1, 2, \dots, N+1$ and letting

$$\begin{aligned} z_i &= (1 - \lambda_{\min,i} - \lambda_{f,i} + \lambda_{\min,i} \lambda_{f,i}) \bar{z}_i \\ &+ (\lambda_{\min,i} + \lambda_{f,i} - \lambda_{\min,i} \lambda_{f,i} - \lambda_{d,i}) \bar{z}_i \\ &+ \lambda_{d,i} \bar{z}_{\min\{1, i-1\}}, \end{aligned} \quad (19)$$

some convex sets of \mathcal{M} can be extracted as

$$Z_i = \{z_i \mid (19), 0 \leq \lambda_{d,i} \leq \lambda_{f,i} \leq 1\}, 1 \leq i \leq N+1. \quad (20)$$

Fig. 2 above illustrates the construction and geometric interpretation of $Z_i[1 : 2]$, $\lambda_{\min,i}$, $\lambda_{f,i}$ and $\lambda_{d,i}$.

Although the convexity of these extracted sets are guaranteed, the non-feasibility may remain. To further ensure the feasibility, linear inequality constraints on $\lambda_{f,i}$, $\lambda_{d,i}$ are introduced as

$$\lambda_{d,i} \leq k_i \lambda_{f,i}, \quad (21)$$

where $0 \leq k_i \leq 1$ is pre-selected to keep the convexified area out of obstacles. Define

$$\begin{aligned} \lambda_f &:= (\lambda_{f,1}, \lambda_{f,2}, \dots, \lambda_{f,N+1})^\top, \\ \lambda_d &:= (\lambda_{d,1}, \lambda_{d,2}, \dots, \lambda_{d,N+1})^\top, \end{aligned}$$

and let

$$J_s(\lambda_f, \lambda_d; \rho) := J(z_i, u_i) + \rho \cdot \|z_0 - z_f\| \|\lambda_f - \mathbf{1}\|^2 \quad (22)$$

with the weighting parameter $\rho \geq 0$, then the corresponding strict problem can be formulated as $\mathcal{P}_s(z_0; N; A(z_0), B(z_0))$:

$$\begin{aligned} \min_{\{\lambda_f, \lambda_d\}} \quad & J_s(\lambda_f, \lambda_d; \rho) \\ \text{s.t.} \quad & 0 \leq \lambda_{f,i} \leq 1, \\ & (12) - (14), (17), (21). \end{aligned} \quad (23)$$

According to (19) and the given dynamics, the right hand side of (22) is also a function of λ_f, λ_d .

For given $\mathcal{P}'_1(z_0; N; A(z_0), B(z_0))$, we now examine the solvability of the corresponding $\mathcal{P}_r(\cdot), \mathcal{P}_s(\cdot)$. Clearly, if $\mathcal{P}'_1(z_0; N; A(z_0), B(z_0))$ is solvable, then $\mathcal{P}_r(z_0; N; A(z_0), B(z_0))$ is also solvable since it has a relaxed constraint set. On other hand, $\mathcal{P}_s(z_0; N; A(z_0), B(z_0))$ is solvable if $\{\bar{z}_1, \dots, \bar{z}_{N+1}; \bar{u}_1, \dots, \bar{u}_N\}$ satisfies the constraints of $\mathcal{P}'_1(\cdot)$ — that is, when $\lambda_f = \mathbf{0}$ and $\lambda_d = \mathbf{0}$. However, if $\mathcal{P}'_1(z_0; N; A(z_0), B(z_0))$ is unsolvable, specific challenges may occur, which we refer to as connective infeasibility as formalized in Definition 1.

Definition 1 $\mathcal{P}'_1(z_0; N; A(z_0), B(z_0))$ is said to exhibit **connective infeasibility** when, despite the problem \mathcal{P}_0 being solvable, either the relaxed or strict problem derived from $\mathcal{P}'_1(z_0; N; A(z_0), B(z_0))$ becomes unsolvable.

Connective infeasibility may occur when the terminal state z_{N+1} simultaneously satisfies: (1) the positional proximity to obstacles ($z_{N+1}[1 : 2]$ near obstacle boundaries), and (2) the conflicting dynamics (significant velocity toward obstacles). To mitigate the connective infeasibility, the term ρ is introduced in $\mathcal{P}_s(\cdot)$ to enhance the robustness, where it is referred to as the safety term. Based on the preceding developments, our solution framework can be summarized in Fig. 3 below.

3.2 Entire Algorithm

The entire algorithm of our proposed method is represented as Algorithm 1. In Algorithm 1 and subsequent analysis, we use superscription $(\cdot)^{(K)}$ to represent problems, relative variables and parameters in the K^{th} planning cycle. To be detailed, let $\mathcal{P}_{(\cdot)}^{(K)}, \mathcal{P}_1^{(K)}$ be the abbreviation of $\mathcal{P}_{(\cdot)}(z_0^{(K)}; N^{(K)}; A^{(K)}, B^{(K)}), \mathcal{P}'_1(z_0^{(K)}; N^{(K)}; A^{(K)}, B^{(K)})$. $\bar{z}_i^{(K)} (\bar{u}_i^{(K)})$ and $\tilde{z}_i^{(K)} (\tilde{u}_i^{(K)})$ are derived from $\mathcal{P}_r^{(K)}$ and a feasible solution of the K^{th} planning cycle respectively by searching algorithm. $\{\lambda_f^{(K)}, \lambda_d^{(K)}\}$ is the optimizer of $\mathcal{P}_s^{(K)}$, while $z_i^{(K)}, u_i^{(K)}$ are computed from $\{\lambda_f^{(K)}, \lambda_d^{(K)}\}$. Algorithm 1 follows a concise iterative structure: it solves the current planning cycle, updates the initial state z_0 using the resulting solution, and proceeds to construct and solve the next planning cycle. This iterative process continues until the quit condition (15) is reached. In this process, the entire control is obtained by sequentially concatenating $\{u_1^{(i)}, \dots, u_{N^{(i)}}^{(i)}\}, i =$

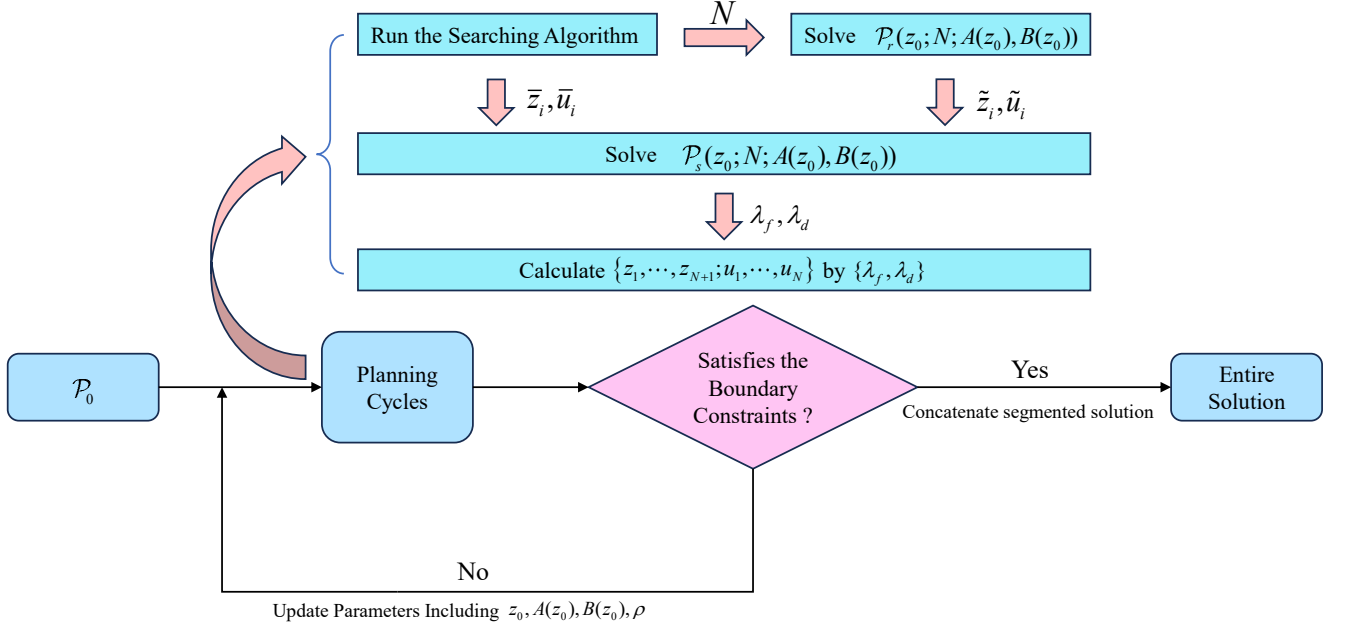


Fig. 3. Processes solving \mathcal{P}_0 in the proposed framework

Algorithm 1 Online Programming Algorithm

```

1: Input: The map information  $\mathcal{M}$ .
2:  $K \leftarrow 1$ ;
3: while  $\|z_{N(K)+1} - z_f\|_{Q_0} \geq \gamma$  do
4:   Get Current State  $z_0^{(K)}$ 
5:   Get a Collision Free Solution  $F^{(K)} := \{z_1^{(K)}, \dots, z_{N(K)+1}^{(K)}; \tilde{u}_1^{(K)}, \dots, \tilde{u}_{N(K)}^{(K)}\}$  through
      Searching Algorithm
6:   Generate the relaxed QCQP Problem
       $\mathcal{P}_r^{(K)}(z_0^{(K)}; N^{(K)}; A^{(K)}, B^{(K)})$ 
7:   Get the solution of  $\mathcal{P}_r^{(K)}(\cdot)$ 
8:   Solve Problem  $\mathcal{P}_s^{(K)}(z_0^{(K)}) \rightarrow \{\lambda_f^{(K)}, \lambda_d^{(K)}\}$ 
9:   Calculate  $\{z_1^{(K)}, \dots, z_{N(K)+1}^{(K)}; u_1^{(K)}, \dots, z_{N(K)}^{(K)}\}$ 
10:  if  $\|z_{N(K)+1} - z_f\|_{Q_0} \geq \gamma$  then
11:    Adjust  $N^{(K)}$  to  $\hat{N}^{(K)}$  with  $\hat{N}^{(K)} < N^{(K)} - 1$ 
       and  $\hat{N}^{(K)} \leq N_{\max}$ 
12:  end if
13:  Apply  $\{u_1^{(K)}, \dots, u_{\hat{N}^{(K)}}^{(K)}\}$ 
14:  Update  $\rho^{(K)}, A^{(K)}, B^{(K)}, w^{(K)}, z_0^{(K)}$ 
15:   $K \leftarrow K + 1$ ;
16: end while

```

1, 2, ..., Note $N^{(K)}$ is initially generated from searching algorithms correspondingly, and subsequently they are used as the problem size in both $\mathcal{P}_r^{(K)}$ and $\mathcal{P}_s^{(K)}$. To maintain the performance of Algorithm 1, the solution of one planning cycle is applied only partially by choosing a smaller $\hat{N}^{(K)}$ and applying $\{u_1, \dots, u_{\hat{N}^{(K)}}\}$. Before proceeding with the algorithm analysis, we will first present two customized trajectory searching algorithms which demonstrate good performance in experiments.

3.3 Customized Vortex Artificial Potential Field

Based on the artificial potential field (APF) [21] method, we propose the Customized Vortex Artificial Potential Field (CVAPF) method as a trajectory search algorithm. Tailored for double-integrator systems, it readily extends to general affine models. Conventional APF simulates a virtual force field to navigate while avoiding obstacles, inspired by physical systems under conservative forces. Its enhancement, the Vortex-APF (VAPF) [22], extends traditional potential fields by incorporating a vortex field that modulate repulsion into rotational patterns, aiding navigation in complex environments. As in both APF and VAPF, the attractive potential is defined as

$$P_{att}(z[1:2]) = \|z[1:2] - z_f[1:2]\|^2. \quad (24)$$

The repulsive potential acts to drive the vehicle away from obstacles, and we formulate it with the form similar to [23] as

$$P_{rep}(z[1:2]) = \zeta \sum_{j=1}^{n_{obs}} \exp \left(\frac{-\beta \cdot (\|z[1:2] - p_j\| - r_j)}{r_j} \right), \quad (25)$$

where β and ζ are pre-selected positive weights. For the APF algorithm, the moving direction can be obtained instantly by calculating $-(\nabla P_{att} + \nabla P_{rep})$ directly. For the VAPF algorithm, the vortex field $E_v(z[1:2])$ is orthogonal to $\nabla P_{rep}(z[1:2])$. Its direction $\mathbf{d}(z[1:2])$ is selected from the unit set

$$\mathcal{D}(z[1:2]) := \left\{ \tilde{\mathbf{d}} \in \text{Null}(\nabla P_{rep}(z[1:2])) \mid \|\tilde{\mathbf{d}}\| = 1 \right\}.$$

The field magnitude is scaled by ζ_v , giving $E_v(z[1:2]) = \zeta_v \mathbf{d}(z[1:2])$. In a 2D map, the set $\mathcal{D}(\cdot)$ contains at least two

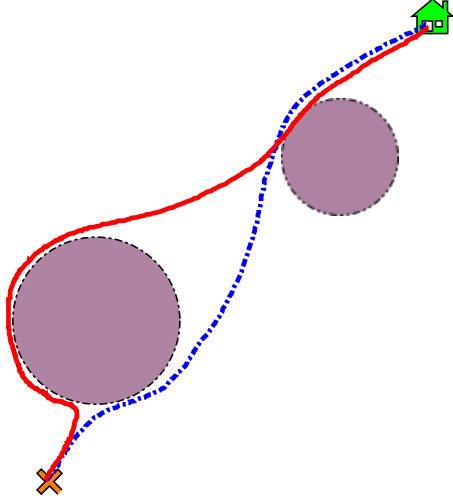


Fig. 4. The solid red line and the dashed blue line represent two possible paths on a map. However, sharp turns in the red path typically signal that the vehicle is slowing down at those points, leading to longer travel times and lower solution quality.

candidate directions. When $\nabla P_{rep}(z[1 : 2]) = \mathbf{0}$, the direction $\mathbf{d}(z[1 : 2])$ may be chosen as any unit vector. By incorporating additional directional selection criteria [24]—rather than restricting to a single turning direction as in [25]—the VAPF algorithm can achieve improved path quality. For instance, it could help to find a shorter way when avoiding an obstacle in the forward of the vehicle, as shown in Fig.2. Denote the expected subsequent moving direction of point \tilde{z}_i as $E_{\tilde{z}_i}^\dagger$, then the VAPF algorithm calculates

$$E(\tilde{z}_i[1 : 2]) = -(\nabla P_{att}(\tilde{z}_i[1 : 2]) + \nabla P_{rep}(\tilde{z}_i[1 : 2])) + E_v(\tilde{z}_i[1 : 2]),$$

and

$$E^\dagger(\tilde{z}_i[1 : 2]) = \frac{E(\tilde{z}_i[1 : 2])}{\|E(\tilde{z}_i[1 : 2])\|}.$$

The vortex field mitigates local minima issues common in APF [26], [27], enabling smoother navigation in complex environments.

To further ensure dynamic feasibility, CVAPF introduces a speed search step: once a direction is selected, feasible speeds consistent with physical constraints are computed. If available, a velocity combining direction and admissible speed is chosen; otherwise, a safe deceleration is applied to slow the vehicle while steering it toward the target direction. The complete CVAPF procedure is outlined in Algorithm 2. In Algorithm 2, a_{safe} is utilized to lower the speed of the agent and alter its direction. Since

$$\begin{aligned} \|a_{safe}\| &= \left\| a_1 E^\dagger(\tilde{z}_{i+1}[1 : 2]) - a_0 \frac{\tilde{z}_i[3 : 4]}{\|\tilde{z}_i[3 : 4]\|} \right\| \\ &\leq \left\| a_1 E^\dagger(\tilde{z}_{i+1}[1 : 2]) \right\| + \left\| a_0 \frac{\tilde{z}_i[3 : 4]}{\|\tilde{z}_i[3 : 4]\|} \right\| \\ &= a_1 + a_0, \end{aligned}$$

$a_{safe} \leq a_{\max}$ can be easily guaranteed by selecting a_1 and a_0 with $a_0 + a_1 \leq a_{\max}$.

Algorithm 2 Customized VAPF Algorithm

```

1: Input: Map Information  $\mathcal{M}$ , Current state  $z_0^{(K)}$ ,  

   speed and accelerations  $v_{\max}, a_{\max}$ .  

    $N \leftarrow 0; \tilde{z}_0 \leftarrow z_0^{(K)}$ ;  

2: while (( $N < N_{\min}$  or Not_Safe) and  $N \leq N_{\max}$ )  

   do  

3:    $\tilde{z}_{N+1} = \tilde{z}_N[1 : 2] + \tilde{z}_N[3 : 4] \cdot \Delta t$   

4:   Calculate  $E(\tilde{z}_{N+1}[1 : 2]), E^\dagger(\tilde{z}_{N+1}[1 : 2])$   

5:   Search a speed  $s_{N+1}$  from  $v_{\max} \rightarrow 0$  which meets  

   the constraints with the moving direction  

6:   if Search is successful then  

7:      $\tilde{z}_{N+1}[3 : 4] = s_{N+1} E^\dagger(\tilde{z}_{N+1}[1 : 2])$   

8:   else  

9:      $a_{safe} = [a_1 E^\dagger(\tilde{z}_{N+1}[1 : 2]) - a_0 \frac{\tilde{z}_N[3 : 4]}{\|\tilde{z}_N[3 : 4]\|}]$   

10:     $\tilde{z}_{N+1}[3 : 4] = \tilde{z}_N[3 : 4] + a_{safe} \cdot \Delta t$   

11:   end if  

12:   Update  $\zeta_v$   

13:   Update Not_Safe  

    $N \leftarrow N + 1$   

14: end while  

15: if Not_Safe = 1 then  

16:   Algorithm Failed;  

17: else  

18:   Calculate  $\{\tilde{u}_1, \tilde{u}_2, \dots\}$   

19:   Return Feasible Trajectory  $F^{(K)}$   

20:   Return  $N^{(K)} \leftarrow N$   

21: end if

```

The N determined by Algorithm 2 is critical in generating high-quality trajectories, as larger values of N correspond to longer period and further compromise both real-time performance and solution accuracy. Moreover, we have found that having the trajectory searching algorithm terminate at a safer position is helpful to enhance the robustness, for instance, the connective infeasibility can greatly be mitigated. On this basis, Algorithm 2 introduces a **Not_Safe** sign. Define

$$T_s := \left\{ t \in [0, t_w] \mid z_{N+1}[1 : 2] + z_{N+1}[3 : 4]t \in \bigcup_{i=1}^{n_{obs}} \mathcal{B}_i \right\},$$

then **Not_Safe** is given by

$$\text{Not_Safe} = \begin{cases} 0, & T_s = \emptyset, \\ 1, & \text{else,} \end{cases}$$

and $\min T_s$ is also a vital parameter used in the updating of $\rho^{(K)}$, where a smaller $\min T_s$ requires bigger $\rho^{(K)}$. Since $N^{(K)}$ generated in Algorithm 2 can be large, adjusting $N^{(K)}$ is meaningful to maintain the precision. These steps also show the necessity to substitute $N^{(K)}$ with $\hat{N}^{(K)}$ in Algorithm 1. Therefore, N_{\max} is further introduced to confine the length of applied control input.

3.4 Customized Dynamic Window Approach

The Customized Dynamic Window Approach (CDWA) is designed as another searching algorithm for nonlinear models based on dynamic window approach (DWA) [28]. By judiciously balancing the trade-offs between speed and safety,

DWA enables agents to navigate dynamic environments with minimal risks. The DWA centers on the concept of a “dynamic window.” This window represents the set of feasible control inputs available to an agent in its current state. Its construction incorporates multiple state factors, including position, orientation, and velocity. System-specific constraints are also integral to this formulation. From the agent’s perspective, it is essential to predict proper actions based on its current state—i.e., to construct a dynamic window. From the algorithm designer’s standpoint, defining a policy to select actions from these feasible sets is equally critical.

In order to apply DWA effectively in our work, the CDWA is proposed. Following the general DWA methods, we first identify the dynamic window at the current state, which is achieved by calculating the possible control inputs based on constraints. Next, a subset of these feasible inputs is extracted for evaluation according to the map information, accompanied with `Not_Safe` flag and $\min T_s$. The state of the next time step is instantly anticipated using the chosen input while refreshing the current state by the anticipated state in the end. Repeat these processes several loops to ultimately generate a trajectory consisting of N inputs and $N+1$ states. The pseudo-code of our proposed CDWA is demonstrated in Algorithm 3 below.

Algorithm 3 Customized DWA Searching Algorithm

- 1: Input: Map information \mathcal{M} , state z_0 .
- 2: $N \leftarrow 1$;
- 3: **while** $((N < N_{\min} \text{ or } \text{Not_Safe}) \text{ and } N \leq N_{\max})$ **do**
- 4: Detect Obstacles along the direction of current velocity
- 5: Calculate the dynamic window
- 6: Obtain $\min T_s$
- 7: Obtain current input
- 8: Update `notsafe`
- 9: $N \leftarrow N + 1$
- 10: **end while**
- 11: Do steps 15-21 in Algorithm 2

3.5 Theoretical Guarantees

We subsequently show the convergence property of Algorithm 1 in a mild assumption given in Assumption 3.

Assumption 3 *there exists a contraction factor $0 \leq \kappa < 1$, which makes*

$$\frac{J_s(\lambda_f^{(K)}, \lambda_d^{(K)}; \rho^{(K)})}{J_s(\lambda_f^{(K-1)}, \lambda_d^{(K-1)}; \rho^{(K-1)})} \leq \kappa \quad (26)$$

hold for all but finitely many iterations K . In other words, the number of iterations that violate (26) is limited.

We discuss two complementary circumstances to explain the reasonableness of Assumption 3. For the Case I, consider that $J_s(\lambda_f^{(K-1)}, \lambda_d^{(K-1)}; \rho^{(K-1)}) \gg \gamma$. Under this precondition, the cost from velocity can be set to a relatively small level if a Q_0 is chosen properly, and the cost function is then mainly decided by the position. Thus, $J_s(\lambda_f^{(K+1)}, \lambda_d^{(K+1)}; \rho^{(K+1)}) \leq J_s(\lambda_f^{(K)}, \lambda_d^{(K)}; \rho^{(K)})$ is naturally satisfied with the assistance of the searching algorithm if the initial velocity $z_0^{(K)}[3:4]$ remains moderate.

On the other hand, if the initial velocity is undesirable, e.g. the vehicle moves away from the target area at maximum speed, it can still achieve (26) after several cycles. Moreover, when encountering obstacles, the vehicle necessitates strategic decision-making regarding its directional maneuver. Since all the obstacles are circle-like, there exists at least one direction that makes the vehicle get closer to the target area. The search algorithm can prioritize this direction. Experiments also show the mildness of Case I. Case II is complementary to Case I. When $J_s(\lambda_f^{(K-1)}, \lambda_d^{(K-1)}; \rho^{(K-1)}) \gg \gamma$ is not satisfied, properly readjusting $\rho^{(K)}$ can drive the vehicle to meet the boundary constraint according to the convexity property of \mathcal{P}_s if the trajectory searching algorithm can divert the vehicle to the target area. Thus, Assumption 3 is moderate. Combined with Assumption 1, it can be proven that the target area is reachable within limited planning cycles, as demonstrated in Theorem 1.

Theorem 1 *For given γ , $z_{N+1}^{(K+1)}$ can be obtained with $\|z_{N+1}^{(K+1)} - z_f\|_{Q_0} \leq \gamma$ after executing finite planning cycles.*

Proof. Under Assumption 4, suppose (26) is violated at the planning cycle K_1, K_2, \dots, K_m , and we define

$$\kappa_i = \frac{J_s(\lambda_f^{(K_i+1)}, \lambda_d^{(K_i+1)}; \rho^{(K_i+1)})}{J_s(\lambda_f^{(K_i)}, \lambda_d^{(K_i)}; \rho^{(K_i)})}. \quad (27)$$

Apparently, $K_m + 1$ cannot be the last iteration. For any $K \geq K_m$, we have

$$\prod_{i=1}^K \frac{J_s(\lambda_f^{(i+1)}, \lambda_d^{(i+1)}; \rho^{(i+1)})}{J_s(\lambda_f^{(i)}, \lambda_d^{(i)}; \rho^{(i)})} \leq \kappa^{K-m} \cdot \prod_{i=1}^m \kappa_i. \quad (28)$$

Since $\|z_{N+1}^{(K+1)} - z_f\| \geq \gamma$ keeps true during each planning cycle except the last one, $J_s(\lambda_f^{(K)}, \lambda_d^{(K)}; \rho^{(K)}) \geq \gamma$ is then consistently satisfied, which indicates that $\kappa_i \leq J_s(\lambda_f^{(K_i+1)}, \lambda_d^{(K_i+1)}; \rho^{(K_i+1)})/\gamma$ are too bounded for any κ_i . Consequently, we have

$$\begin{aligned} \|z_{N+1}^{(K+1)} - z_f\|_{Q_0} &\leq J_s(\lambda_f^{(K+1)}, \lambda_d^{(K+1)}, \rho^{(K+1)}) \\ &\leq J_s(\lambda_f^{(1)}, \lambda_d^{(1)}, \rho^{(1)}) \kappa^{K-m} \cdot \prod_{i=1}^m \kappa_i. \end{aligned} \quad (29)$$

Take

$$K > \frac{\left(\log \frac{\gamma}{J_s(\lambda_f^{(1)}, \lambda_d^{(1)}, \rho^{(1)})} - \sum_{i=1}^m \log \kappa_i \right)}{\log \kappa} + m, \quad (30)$$

then $\|z_{N^{(K)}+1}^{(K+1)} - z_f\|_{Q_0} \leq \gamma$ holds after executing K planning cycles, thereby completes the proof. \square

Building upon Theorem 1, we will further establish the sufficient condition for the local optimality property of the concatenated solution. Here, two assumptions are required for further analysis, which is demonstrated as Assumptions 4-5.

Assumption 4 *In the subsequent analysis, for each planning cycle $\mathcal{P}_1'(z_0^{(K)}; N^{(K)}; A^{(K)}, B^{(K)})$, $B^{(K)}$ has full column rank. For the corresponding problem $\mathcal{P}_1(z_0^{(K)}; N^{(K)})$, the Jacobian matrix $(\frac{\partial f}{\partial u})^\top$ evaluated at the optimizer is also of full column rank.*

Remark 2 Assumption 4 is both important and mild. For a full-column-rank Jacobian $(\frac{\partial f}{\partial u})^\top$, we have $(\frac{\partial f}{\partial u})^\top v = 0 \Rightarrow v = 0$ for any relevant vector v , which is crucial in subsequent theoretical proofs. Moreover, this condition is naturally satisfied in most underactuated systems, aligning well with practical engineering applications.

We further introduce $\mathcal{L}_2(z_0; \cdot), \mathcal{L}_3(z_0; \cdot), \dots$ to denote the Lagrangian function of $\mathcal{P}_1(z_0; N; \cdot)$. Namely, in $\mathcal{P}_1(z_0; N)$, we define

$$\begin{aligned} \mathcal{L}_N(z_0; z_i, u_i, v_i, \zeta_{ij}, s_i, q_i) := & \|z_{N+1}\|_{Q_0}^2 \\ & + \sum_{i=1}^N v_i (z_{i+1} - f(z_i, u_i)) \\ & + \sum_{i=1}^{N+1} \sum_{j=1}^{n_{obs}} \zeta_{ij} (r_j^2 - \|z_i[1:2] - p_j\|^2) \\ & + \sum_{i=1}^{N+1} s_i G_1(z_i) + \sum_{i=1}^N q_i G_2(u_i), \end{aligned} \quad (31)$$

where $v_i, \zeta_{ij}, s_i, q_i$ are Lagrange multipliers.

Assumption 5 The local optimizer of $\mathcal{P}_1(z_0; N)$ (if exists) satisfies the Mangasarian–Fromovitz constraint qualification (MFCQ) [29]. Specifically, at such a optimizer, the gradients of all active equality constraints are linearly independent, and there exists a vector that is:

- 1). a descent direction for all active inequality constraints;
- 2). orthogonal to the gradients of all equality constraints.

Under Assumption 5, if $\mathcal{P}_1(\cdot)$ admits a local optimizer, then there exists a pair of Lagrange multipliers such that the optimizer satisfies the Karush–Kuhn–Tucker (KKT) conditions. This result further leads to Theorem 2.

Theorem 2 Suppose $\mathcal{P}_1(z_0; m)$ has a local optimizer $\{z_1^1, z_2^1, \dots, z_{m+1}^1; u_1^1, \dots, u_m^1\}$. For any $m' \leq m-1$, if $\{z_1^2, z_2^2, \dots, z_{n+1}^2; u_1^2, \dots, u_n^2\}$ is a local optimizer of $\mathcal{P}_1(z_{m'+1}^1; n)$, $u_1^2{}^\top Q_2 u_1^2 < 1$ and $u_{m'+1}^1{}^\top Q_2 u_{m'+1}^1 < 1$, then

$$\{z_1^1, \dots, z_{m'}^1, z_1^2, \dots, z_{n+1}^2; u_1^1, \dots, u_{m'}^1, u_1^2, \dots, u_n^2\}$$

satisfies the KKT conditions of $\mathcal{P}_1(z_0; m' + n)$ with the corresponding multipliers.

Proof. See Appendix A. \square

For the approximated problem $\mathcal{P}'_1(\cdot)$, we can analogy show the reasonableness of solution concatenate when using approximated dynamics; this is demonstrated in Corollary 1.

Corollary 1 Suppose $\{z_1^1, \dots, z_{m+1}^1; u_1^1, \dots, u_m^1\}$ locally solves a variant of $\mathcal{P}'_1(z_0; m; \cdot)$, with the dynamic constraints changed as $z_{i+1} = A_i^1 z_i + B_i^1 u_i + w_i^1$, and $\{z_1^2, \dots, z_{n+1}^2; u_1^2, \dots, u_n^2\}$ locally solving an variant of $\mathcal{P}'_1(z_{m'+1}^1; n; \cdot)$, where the dynamics are substituted by $z_{i+1} = A_i^2 z_i + B_i^2 u_i + w_i^2$. Then,

$$\{z_1^1, \dots, z_{m'+1}^1, z_2^2, \dots, z_{n+1}^2; u_1^1, \dots, u_{m'}^1, u_2^2, \dots, u_n^2\}$$

locally solves a variant of $\mathcal{P}'_1(z_0; m' + n, \cdot)$, where the corresponding constraint matrices are substituted by

$$(A_i, B_i, w_i) = \begin{cases} (A_i^1, B_i^1, w_i^1), & i \leq m', \\ (A_{i-m'}^2, B_{i-m'}^2, w_{i-m'}^2), & i > m' \end{cases}$$

as long as the following conditions are satisfied:

- 1). the constraints $u_{m'}^1{}^\top Q_2 u_{m'}^1 < 1, u_{m'+1}^1{}^\top Q_2 u_{m'+1}^1 < 1$ and $u_{m'+1}^2{}^\top Q_2 u_{m'+1}^2 < 1$ hold simultaneously;
- 2). the matrices $B_{m'}^1, B_{m'+1}^1$ and B_1^2 are of full column rank.

Theorem 2 and Corollary 1 reveal the soundness of concatenating segmented control inputs and further illuminate the rule of adjusting $N^{(K)}$. Although we only considered concatenating 2 segments in the analysis, it is easy to extend the conclusion to multiple trajectory synthesis cases. Moreover, in some specific cases, the aforementioned trajectory synthesizing method can reliably identify the global optimal trajectory, even when dealing with non-convex constraint sets. The result is established in Theorem 3.

Theorem 3 Under the notations and conditions of Theorem 2, solve $\mathcal{P}_1(z_0; \cdot), \mathcal{P}_1(z_{m'+1}^1; \cdot)$ by Algorithm 1. If f is further affine and the corresponding λ_{\min} of $\mathcal{P}_s(z_0; \cdot)$ and $\mathcal{P}_s(z_{m'+1}^1; \cdot)$ are all zero, then

$$\{z_1^1, \dots, z_{m'}^1, z_1^2, \dots, z_{n+1}^2; u_1^1, \dots, u_{m'}^1, u_1^2, \dots, u_n^2\}$$

globally solves $\mathcal{P}_1(z_0; m' + n)$.

Proof. Since f is affine, we have $\mathcal{P}_1(z_0; m' + n) = \mathcal{P}'_1(z_0; m' + n; \frac{\partial f}{\partial z_0}^\top, \frac{\partial f}{\partial u}^\top)$ for any z_0 . Let us recall $\mathcal{P}_r(z_0; m' + n; A, B)$ following

$$\begin{aligned} \min_{\{Z; U\}_N} & (z_{m'+n+1} - z_f)^\top Q_0 (z_{m'+n+1} - z_f) \\ \text{s. t.} & (12) - (14), (17). \end{aligned}$$

If all the corresponding $\lambda_{\min,i} \equiv 0$, then for both of $\mathcal{P}'_1(z_0; m; \cdot)$ and $\mathcal{P}'_1(z_{m'+1}^1; n; \cdot)$, the corresponding optimizer coincide with those of $\mathcal{P}_r(z_0; m; \cdot)$ and $\mathcal{P}_r(z_{m'+1}^1; n; \cdot)$ respectively. Hence, we can conclude that

$$\{z_1^1, \dots, z_{m'}^1, z_1^2, \dots, z_{n+1}^2; u_1^1, \dots, u_{m'}^1, u_1^2, \dots, u_n^2\}$$

is also the optimizer of $\mathcal{P}_r(z_0; m' + n; \cdot)$. With the convexity of $\mathcal{P}_r(\cdot)$, it can further prove the global optimality of the concatenated solution. Since the global optimal solution of $\mathcal{P}_r(z_0; m' + n; \cdot)$ has a lower or equal cost of $\mathcal{P}'_1(z_0; m' + n; \cdot)$, it can be obtained that the concatenated solution is also the global optimizer of $\mathcal{P}'_1(z_0; m' + n; \cdot)$. This completes the proof. \square

The aforementioned analysis can be readily extended to scenarios involving the concatenation of solutions across multiple planning cycles. Indeed, these theoretical results demonstrate the validity of iteratively solving each $\mathcal{P}'_1(z_0^{(K)}; N^{(K)}, A^{(K)}, B^{(K)})$ in Algorithm 1. In the subsequent discussion, we discuss another critical index: time cost of the entire control. Given that our discretization is based on fixed step lengths, Algorithm 1 utilizes $\hat{N}^{(K)}$ from its planning cycles to profile time cost. In fact, we can obtain the final time of entire control as $t_f = h \sum_{i=1}^{K-1} \hat{N}^{(i)} + h \hat{N}^{(K)}$. Since $h \hat{N}^{(K)} \leq h N_{\max}$, one can obtain a preciser evaluation of t_f by applying a smaller $N_{\max} h$. However, it is unnecessary to calculate an accurate t_f to present the “time-optimality” of the entire control. Instead, we could demonstrate that t_f is achieved approximately to local minimal final time. To show this claim, suppose that $\{z_1^{(j)}, \dots, z_{\hat{N}^{(K)}+1}^{(j)}\}$ are extracted from solving $\mathcal{P}'_1(z_0^{(1)}; \cdot), \mathcal{P}'_1(z_0^{(2)}; \cdot), \dots, \mathcal{P}'_1(z_0^{(K)}; \cdot)$,

and that the solution of $\mathcal{P}'_1(z_0^{(K)}; \cdot)$ satisfies the quit condition of Algorithm 1; then, we have $\hat{N}^{(K)} = N^{(K)}$. If $\{z_1^{(1)}, \dots, z_{N^{(K)}+1}^{(K)}; u_1^{(1)}, \dots, u_{N^{(K)}}^{(K)}\}$ is a local optimal solution of $\mathcal{P}_1(z_0^{(1)}; h \sum_{i=1}^{K-1} \hat{N}^{(i)} + h \hat{N}^{(K)}; \cdot)$, then there exists a neighbor scaled by δ for arbitrary $\{z_1^{(1)}(\delta), \dots, z_{N^{(K)}+1}^{(K)}(\delta); u_1^{(1)}(\delta), \dots, u_{N^{(K)}}^{(K)}(\delta)\}$ satisfying all of the constraints of $\mathcal{P}_1(\cdot)$. We further have

$$\|z_{N^{(K)}+1}^{(K)}(\delta) - z_f\|_{Q_0}^2 \geq \|z_{N^{(K)}+1}^{(K)} - z_f\|_{Q_0}^2.$$

If it further holds $(z_{N^{(K)}+1}^{(K)}(\delta) - z_f)^\top Q_0 (z_{N^{(K)}+1}^{(K)}(\delta) - z_f) \geq \gamma^2$, Algorithm 1 will continue with at least one planning cycle. In this circumstance, suppose $U(\delta) = \{u_1^{(1)}(\delta), \dots, u_{N+1}^{(K)}(\delta), \dots\}$ is an available control of \mathcal{P}_0 , then it can be obtained that $t_f(\delta) - t_f \geq h$ with $t_f(\delta)$ the final time of using $U(\delta)$. Otherwise, if $(z_{N^{(K)}+1}^{(K)}(\delta) - z_f)^\top Q_0 (z_{N^{(K)}+1}^{(K)}(\delta) - z_f) \leq \gamma^2$, then we have $t_f(\delta) = t_f$. The tendency toward local optimal solutions becomes more pronounced with shorter time horizons. To show this, we rewrite the quit condition to an equivalent form as

$$\|z_{N^{(K)}+1}^{(K)} - z_f\|_{Q_0}^2 \leq \gamma^2. \quad (32)$$

Then, we have

$$\|z_{N^{(K)}+1}^{(K)} - z_f\|_{Q_0}^2 - \|z_{N^{(K)}+1}^{(K-1)} - z_f\|_{Q_0}^2 \quad (33)$$

$$\leq 2\|z_1^{(1)} - z_f\| \|z_{N^{(K)}+1}^{(K)} - z_{N^{(K)}+1}^{(K-1)}\| \|Q_0\|_2 \quad (34)$$

$$\begin{aligned} &\leq 2\|z_1^{(1)} - z_f\| \cdot \left(\|z_{N^{(K)}+1}^{(K)} - z_{\hat{N}^{(K-1)}+1}^{(K-1)}\| \right. \\ &\quad \left. + \|z_{\hat{N}^{(K-1)}+1}^{(K-1)} - z_{N^{(K)}+1}^{(K-1)}\| \right) \cdot \|Q_0\|_2. \end{aligned} \quad (35)$$

For $\|z_{N^{(K)}+1}^{(K)} - z_{\hat{N}^{(K-1)}+1}^{(K-1)}\|$, we can further obtain

$$\begin{aligned} &\|z_{N^{(K)}+1}^{(K)} - z_{\hat{N}^{(K-1)}+1}^{(K-1)}\| \\ &= \|z_{N^{(K)}+1}^{(K)} - z_1^{(K)}\| \\ &\leq \sum_{i=1}^{N^{(K)}} \|z_{i+1}^{(K)} - z_i^{(K)}\| \\ &= h \cdot \underbrace{\sum_{i=1}^N \|A_c(z_0^{(K)})z_i^{(K)} + B_c(z_0^{(K)})u_i^{(K)} + w_c(z_0^{(K)})\|}_M \\ &\leq N_{\max}h \cdot M. \end{aligned} \quad (36)$$

Similarly,

$$\begin{aligned} &\|z_{\hat{N}^{(K-1)}+1}^{(K-1)} - z_{N^{(K)}+1}^{(K-1)}\| \\ &\leq \sum_{i=\hat{N}^{(K-1)}+1}^{N^{(K-1)}} \|z_{i+1}^{(K-1)} - z_i^{(K-1)}\| \\ &\leq N_{\max}h \cdot M. \end{aligned} \quad (37)$$

In the above steps, (34) is a direct result of Assumption 3. With the boundness of $u_i^{(K)}$ and $z_i^{(K)}$, (35), (36) and (37) indicate (33) $\rightarrow 0$ as $N_{\max}h \rightarrow 0$. With $\|z_{N^{(K-1)}+1}^{(K-1)} - z_f\|_{Q_0} > \gamma$ and $\|z_{N^{(K)}+1}^{(K)} - z_f\|_{Q_0} \leq \gamma$, we can obtain $\|z_{N^{(K)}+1}^{(K)} - z_f\|_{Q_0} \rightarrow \gamma^-$ as $N_{\max}h \rightarrow 0$. Hence, we can choose a sufficient small $N_{\max}h$, that making all $\{u_1^{(1)}(\delta), \dots, u_{N+1}^{(K)}(\delta)\}$ failed to meet the quit condition for given δ except for $\{u_1^{(1)}, \dots, u_{N+1}^{(K)}\}$ itself. Thus, $h \sum_{i=1}^K \hat{N}^{(i)}$ converges to a local minimal t_f .

Remark 3 Although $h \sum_{i=1}^K \hat{N}^{(i)}$ converges to a local minimum as $N_{\max}h \rightarrow 0$, some undesired phenomenons may appear if $N_{\max}h$ is too small, e.g. the conditions of Theorem 2 may be difficult to be satisfied. Therefore, t_f can generally approximate to a local minimal final time since a lower bound of $N_{\max}h$ should be added.

Next, some sufficient conditions for the equivalence of solving $\mathcal{P}_s(z_0^{(K)}; N^{(K)}; A^{(K)}, B^{(K)})$ and $\mathcal{P}'_1(z_0^{(K)}; N^{(K)}; A^{(K)}, B^{(K)})$ will be provided. We begin with defining the relative interior solution.

Definition 2 A feasible solution to $\mathcal{P}_s^{(K)}(\cdot)$ is called a relative interior solution if for all $1 \leq i \leq N^{(K)}+1$, the computed position components $z_i^{(K)}[1:2]$ lie in the relative interior of $\mathcal{Z}_i[1:2]$.

Theorem 4 When $\rho^{(K)} = 0$, the corresponding $\{z_1^{(K)}, \dots, z_{N^{(K)}+1}^{(K)}; u_1^{(K)}, \dots, u_{N^{(K)}}^{(K)}\}$ calculated from the optimal solution of $\mathcal{P}_s^{(K)}(z_0^{(K)}; N^{(K)}; \cdot)$ is a local optimizer for $\mathcal{P}'_1(z_0^{(K)}; N^{(K)}; \cdot)$, if at least one of the following two conditions is satisfied:

- 1). all $\lambda_{\min,i}^{(K)} = 0$ or $\tilde{z}_i = \bar{z}_i$, $i \in \{1, \dots, N^{(K)}+1\}$;
- 2). the obtained optimizer of $\mathcal{P}_s^{(K)}$ is a relative interior solution.

Proof. See Appendix B. \square

Remark 4 Theorem 4 requires two preconditions. The first precondition is satisfied when the solution to the corresponding problem $\mathcal{P}_r(\cdot)$ is collision-free. The later holds if the optimizer of $\mathcal{P}'_1(\cdot)$ lies strictly in the generated convex region. In a subset of the map where obstacles are not overly dense, the first precondition is typically met.

We have analyzed properties of Algorithm 1 under the assumption that the safety term is disabled, i.e., $\rho^{(j)} = 0$ in each $\mathcal{P}_s^{(j)}$. We now briefly examine the effect of the safety term. Suppose $\{\lambda_f^*(\rho), \lambda_d^*(\rho)\}$ is an optimal solution of $\mathcal{P}_s(z_0^{(K)}; \cdot)$ with $\rho^{(K)} = \rho$. Then, we can obtain

$$\begin{aligned} J_s(\lambda_f^*(0), \lambda_d^*(0); 0) &\leq J_s(\lambda_f^*(\rho), \lambda_d^*(\rho); \rho), \\ &\leq J_s(\lambda_f^*(0), \lambda_d^*(0); 0) \\ &\quad + \rho \cdot \|z_0^{(K)} - z_f\| \|\lambda_f^*(0) - \mathbf{1}\|^2 \\ &\leq J_s(\lambda_f^*(0), \lambda_d^*(0); 0) \\ &\quad + \rho N_{\max} \|z_0^{(K)} - z_f\|. \end{aligned} \quad (38)$$

To analyze the error derive from the safety term, we need to present two important theorems first, which are demonstrated as Theorem 5 and Theorem 6, respectively.

Theorem 5 Suppose $\Theta : \mathbb{R}^{l_\Theta} \supset \mathbb{E} \mapsto \mathbb{R}$ is a continuous closed convex function with unique optimizer, and the minimum of Θ is denoted by Θ_{opt} . Define $\Phi_\Theta(s) :=$

$\text{diam}(\text{Lev}(\Theta, s))$, then $\Phi_\Theta(s)$ is upper semi-continuous for $s \in [\Theta_{\text{opt}}, \infty)$. Here,

$$\text{Lev}(\Theta, s) = \{\mathbf{x} \mid \Theta(\mathbf{x}) < s\}$$

is the strict sublevel set of Θ at s , and

$$\overline{\text{Lev}}(\Theta, s) = \{\mathbf{x} \mid \Theta(\mathbf{x}) \leq s\}$$

is the sublevel set of Θ at s .

Proof. See Appendix C. \square

Theorem 5 is based on the condition that the optimizer of Θ is unique. If this condition is not satisfied, it can also easily obtain that $\Phi_\Theta(s)$ is upper semi-continuous for $s \in (\Theta_{\text{opt}}, \infty)$ while its upper semi-continuous range changes to $[\text{Lev}(\Theta, \Theta_{\text{opt}}), \infty)$. Using similar mathematical method, we can further prove another important theorem, which is presented as Theorem 6.

Theorem 6 Suppose $\Theta : \mathbb{R}^{l_\Theta} \supset \mathbb{E} \rightarrow \mathbb{R}$ is a closed convex function, and $\mathbb{E} \neq \emptyset$ is a closed convex set. Denote X^* as the optimal set of Θ , where $\Theta(\mathbf{x}^*) = \min\{\Theta(\mathbf{x}) \mid \mathbf{x} \in \mathbb{E}\} := \Theta_{\text{opt}}$ for any $\mathbf{x}^* \in X^*$. If X^* is bounded, then

$$\varphi(s) := \begin{cases} \max_{\mathbf{x} \in \text{Lev}(\Theta, s)} \{\|\text{Proj}_{X^*}(\mathbf{x}) - \mathbf{x}\|\}, & \Theta_{\text{opt}} < s, \\ 0, & \text{else} \end{cases}$$

is upper semi-continuous for $s \in [\Theta_{\text{opt}}, \infty)$, and

$$\lim_{s \rightarrow \Theta_{\text{opt}}^+} \left(\max_{\mathbf{x} \in \text{cl}(\text{Lev}(\Theta, s))} \|\mathbf{x} - \text{Proj}_{X^*}(\mathbf{x})\| \right) = 0, \quad (39)$$

where $\text{Proj}_{X^*}(\mathbf{x}) := \arg \min_{\mathbf{y} \in \mathbb{E}} \{\|\mathbf{y} - \mathbf{x}\| \mid \mathbf{y} \in X^*\}$ is the projection of \mathbf{x} with respect to X^* .

Proof. See Appendix D. \square

Since $\mathcal{P}_s(\cdot)$ is convex, combining (38) we can obtain that as $\rho/\|Q_0\|_2 \rightarrow 0^+$ the difference between $\{\lambda_f^*(\rho), \lambda_d^*(\rho)\}$ and $\{\lambda_f^*(0), \lambda_d^*(0)\}$ converges to 0 according to the conclusion of Theorem 5 and 6. As a result, it is reasonable to consider the solution of $\mathcal{P}_s(\cdot)$ as the optimal solution of $\mathcal{P}'_1(\cdot)$ while ignoring the effect of the safety term, if $\|Q_0\|_2 \gg \rho$ and any of the two cases in Theorem 4 is satisfied.

Despite the aforementioned strict problems can be solved with lower computational burdens, their local optimality condition is not as moderate as initially thought. If a stricter local optimal solution is required, SCP can also be an effective substitution for searching algorithms; that is to use SCP algorithm solving $P_1(z_0^{(K)}, \dots)$ directly rather than $P'_1(z_0^{(K)}, \dots)$. In fact, there are three approaches for solving the control problem: (1) solving each planning cycle in the framework of Algorithm 1; (2) the conventional approach directly addresses the original non-convex problem using either general non-convex optimization techniques or sequential convex programming (SCP) methods; and (3) a hybrid alternative that explicitly solves $\mathcal{P}_1(\cdot)$ with NLP Algorithms.

3.6 Contribution Summary

We now summarize section 3 and the main contributions of our work. Subsections 3.1–3.2 introduce the novel time-optimal MPC method. In 3.3, the proposed CVAPF method employs a novel end-to-end computation framework integrating state and control. It (1) can be directly deployed as

a trajectory planning method, and (2) achieves high robustness through the incorporation the safety acceleration a_{safe} and the condition flag **Not_Safe**. Subsection 3.4 provides theoretical support through two original results—Theorems 2 and 4—which, to the best of our knowledge, represent new contributions to the field. Theorem 2 formalizes the local optimality preservation under trajectory concatenation, while Theorem 4 further establishes the equivalence between solutions of $\mathcal{P}'_1(\cdot)$ over local subsets of \mathcal{M} and those derived in the global configuration space.

4 Numerical Experiments

In this section, some numerical experiments are presented to illustrate the capabilities of Algorithm 1 in both static and time-varying map scenarios. We conduct these experiments using MATLAB 2017a with an Intel Core i7 9th 8GB-RAM with the assistance of the CVX toolbox [30] [31].

4.1 Experiments with Static Maps

In this part, we generate maps with fixed circular obstacles to evaluate the algorithm's capability in static scenarios. The dynamics are chosen as the double integrator model, where the constraint (12), (13) are specialized as $\|z_i[1 : 2]\| \leq v_{\text{max}}$, $\|u_i\| \leq a_{\text{max}}$. Some critical parameters are presented in Table 1.

Table 1
Parameters

Vehicle Parameters	$v_{\text{max}}(\text{m/s})$	$a_{\text{max}}(\text{m/s}^2)$	z_f	$z_0^{(1)}$
Range	12	20	$[160, 160, 0, 0]^\top$	$0_{4 \times 1}$
Map parameters	n_{obs}	$r_i(\text{m})$	$\ell(\text{m})$	γ
Range	20	$[3, 11]$	7	3

During map generation, circular obstacles are randomly placed using a built-in random function with seed 20250712. A validation step ensures both target reachability and compliance with map constraints. To illustrate vehicle performance, we select one map and conduct simulations using Algorithm 1 and comparative SCP algorithms. The resulting trajectories are visualized in Fig. 5.

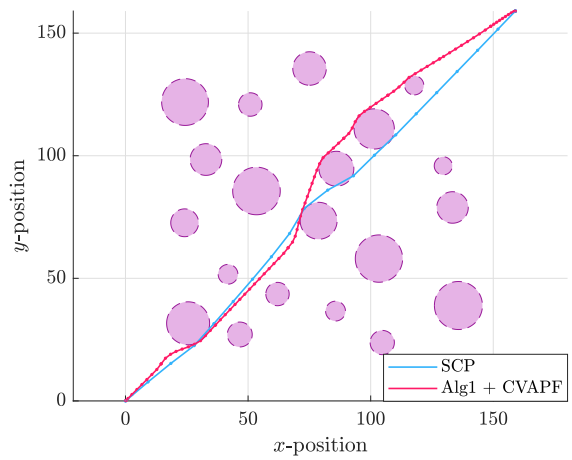


Fig. 5. Trajectories generated by 2 distinct algorithm

In Fig. 5, the red line represents the trajectory of locations obtained using Algorithm 1 with the CVAPF searching algorithm, while the blue line depicts the trajectory of locations obtained by a general sequential convex programming algorithm parameterized with 24 nodes. The trajectory of Algorithm 1 is concatenated by 14 segmented trajectory, while in 12 planning cycles, the precondition of Theorem 4 can be satisfied. Throughout this work, implementations of the SCP algorithm employ a deterministic initialization strategy. During the preparation phase, we set $u_i \equiv 0$ and $z_i = (i-1)\frac{z_f - z_0}{N} + z_0$. This “initial guess” is then refined by running a few SCP iterations with a large trust region, yielding the final initial guess used in subsequent optimization. Notably, both of the two location trajectories are available yet exhibit varying qualities. The numerical characteristics of the two trajectories are listed in TABLE 2.

Table 2
Quality Comparison

	SCP(24 nodes)	Algorithm 1 + CVAPF
t_f (seconds)	20.95	21.12
CT(seconds)	27.80	13.90

Correspondingly, the control inputs are shown in Fig.4. In the two charts, the red dashed line represents the acceleration of the x -direction, while the blue dashed line represents the acceleration of the y -direction. In this experiment, we

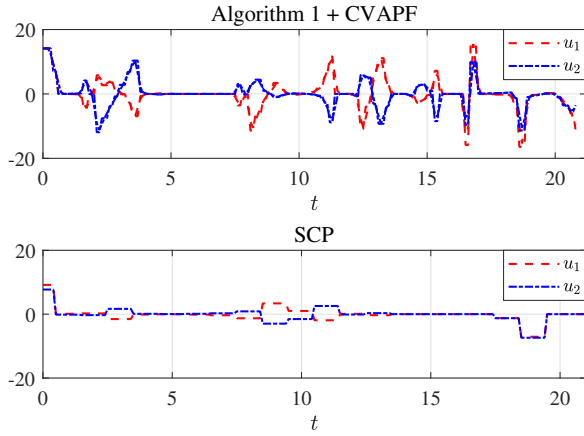


Fig. 6. The inputs generated by distinct algorithms: (1) Algorithm 1 with CVAPF, (2) Comparative SCP Algorithm.

set the SCP algorithm to use 24 nodes since we observed that increasing the number of nodes significantly raises computational cost, while reducing it further leads to substantial loss of accuracy. To further evaluate the capability of Algorithm 1, we employ various metrics in subsequent experiments. Here, we employ the unicycle model, where the feasible trajectory are obtained by CDWA. Specifically, we utilize indexes such as t_f , success rate, and computational time to assess performance. We first test the computation time. In this part, each algorithm is individually tested on 100 maps, with results plotted in Fig. 5 and statistical indicators listed in TABLE 3. In the 1296 planning cycles, there are only 179 planning cycles which is out of the precondition of Theorem 4. For the success rate in TABLE 3,

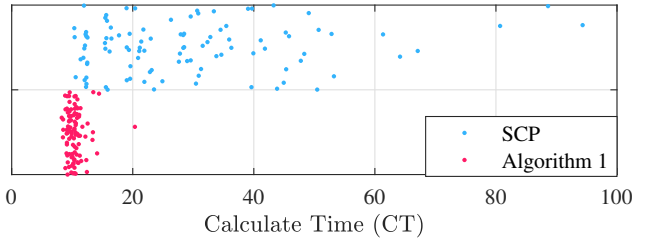


Fig. 7. A comparison of the running time between SCPs and our algorithm

Table 3
Quality Comparison of Distinct Algorithms

	Algorithm 1 + CDWA	SCP
Success Rate(%)	90.1	87.4
CT(Average)	10.40	29.23
CT(Worst)	20.35	94.32
CT(Medium)	10.25	25.60

some clarifications must be presented here. We evaluate a trial “success” if the obtained solution can exactly navigate the vehicle to the target area without violate any obstacle avoidance constraint. It should be noted that the factors contributing to unsuccessful trials differ between our proposed algorithm and baseline methods due to their inherent technical distinctions. As detailed in TABLE 4, we establish separate failure criteria for each algorithm. The “✓” in the table

Table 4
Failure Criteria Comparison

Failure Mode	Algorithm 1	Competed SCP
Infeasibility	✓	✓
Constraint violation	✓	✓
Excessive comp. time	✓	✗

indicates that the occurrence of the corresponding condition is considered an experimental failure when using that particular algorithm. Conversely, “✗” signifies that the specified condition does not constitute a failure criterion for the respective algorithm. The term “Infeasibility” means connective infeasibility and solver infeasibility (namely, the numerical solver cannot run correctly due to no solution exists, ill-conditioned solutions, etc.) for Algorithm 1, while artificial infeasibility and solver infeasibility for Competed SCP. For our proposed framework, the vehicle must complete each planning cycle within this horizon duration to maintain operational continuity, hence excessive computational time of a cycle is not acceptable, while in competed SCP algorithms, this factor is not need to consider. Fig.7 further reveals that Algorithm 1 outperforms SCP algorithms in terms of calculation efficiency, with a shorter average computing time while having a more concentrated distribution of results. In contrast, SCP algorithms exhibit longer computation times

and a more scattered distribution.

4.2 Experiments with Dynamic Maps

In this part, we will conduct experiments to show the robustness of Algorithm 1 in time-varying maps with moving obstacles. First, we revise and add some extra parameters shown in Table 5 to profile a time-varying map.

Table 5

The Parameters included in the experiments with time-varying maps

Vehicle Parameters	v_{\max} (m/s)	a_{\max} (m/s 2)	z_f	$z_0^{(1)}$
Range	6.0	6.0	$[160, 160, 0, 0]^T$	$0_{4 \times 1}$
Map parameters	n	r_i (m)	ϵ (m)	v_o (m/s)
Range	{3, 20}	[3, 11]	7	$0.3v_{\max}$

Here, v_o is applied to depict the maximal speed of obstacles, where for arbitrary $p_i(t)$ there exists $\|p_i(t+\tilde{t}) - p_i(t)\| \leq v_o \cdot |\tilde{t}|$ for any t and \tilde{t} . For clarity, we first demonstrate Algorithm 1 in a toy example with 3 obstacles, as a sparse layout allows clear visualization of its behavioral characteristics. Subsequently, to validate scalability, we test the algorithm in a dynamic scenario containing 20 moving obstacles. To simulate realistic obstacle motion, each obstacle's position is updated via a double-integrator model with saturation. At each simulation step, the current velocity of an obstacle is measured, and—in a manner analogous to the DWA—a feasible set of accelerations consistent with the next velocity is constructed. An acceleration value is then randomly selected (with seed 0) from this set to update the obstacle's state. The obstacle's velocity and position are then updated sequentially through numerical integration. In the example, two figures are plotted to show the specific movement of the vehicle and obstacles in two distinct perspectives, which are demonstrated in Fig. 6.

In Fig.8, both graphs share the same vertical axis, representing the time. When the vertical coordinates are specified, the corresponding horizontal plane represents the danger areas from obstacles at that particular moment. The solid black line indicates the vehicle's trajectory throughout the task. By combining these two charts, it becomes evident that Algorithm 1 effectively avoids obstacles, showcasing its capability with the assistance of searching algorithms in a dynamic map. Furthermore, to aid readers in comprehending the obstacle avoidance capabilities of the vehicle more clearly, we provide a corresponding display diagram as depicted in Fig.9.

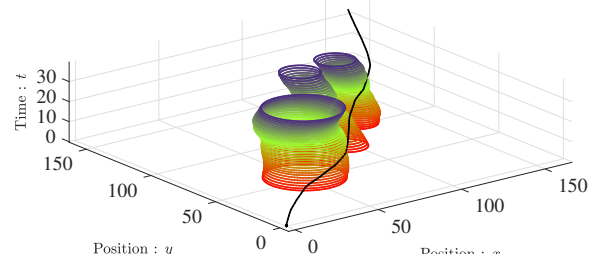
In Fig.7, the minimal distance between the vehicle and danger zones is demonstrated. It shows that the vehicle keeps a distance bigger than 0.2760m from all the danger zones at any time.

With $n = 20$, we conduct subsequent experiments, testing Algorithm 1 with 150 diverse maps. The results are demonstrated in TABLE 6. The last column of TABLE 6 is the rate of planning cycles which satisfies the preconditions of Theorem 4.

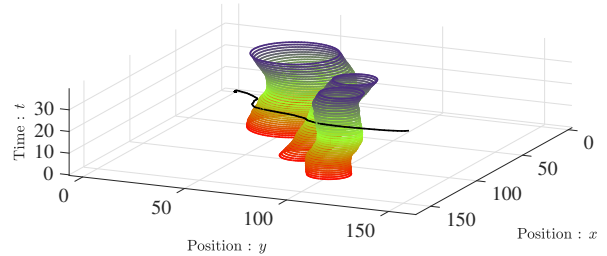
Table 6

Quality Comparison in Time Varying maps

	Success Rate%	CT(Average)	CT(medium)	Rate(%)
Alg1 + CVAPF	90.2	12.8	12.1	78.0
Alg1 + CDWA	91.7	13.0	13.4	79.2



(a) Perspective 1



(b) Perspective 2

Fig. 8. Obstacle avoidance experiment in time-varied scenarios: A Result

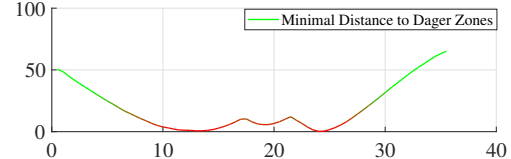


Fig. 9. The minimal distance to danger zones during the task. in this figure, the minimal value is 0.2760

5 Conclusion

Our two-layer optimization-based planning algorithm demonstrated its capability in both theoretical proof and numerical experiments. Specifically, the proposed algorithm generates near time-optimal trajectory with a higher speed while maintain the success rate. The meaning of “near time-optimal” is of three fold. (1) The computed trajectory’s final time must be an integer multiple of the discretization step h . Although the exact local optimum may not be attained, the algorithm performs well with a small h . (2) Despite the use of an approximated affine model, the solution becomes more precise when the system nonlinearity is mild and the planning horizon is sufficiently short. (3) While the preconditions of Theorem 4 may occasionally fail to hold, the resulting trajectories still exhibit near-local-optimal behavior overall.

Moreover, experimental results indicate that occasional violation of these preconditions has limited impact on the final time. However, the model still encounters challenges in extreme scenarios. One key limitation arises from its discrete solution generation, which only guarantees the feasibility in given discrete time points. As a result, it may struggle with feasibility at interpolated states, which is also a common issue faced by general motion planning algorithms. When the planning horizon for a single cycle is excessively long, the timeliness of solutions is compromised, and the algorithm may fail in dynamic scenarios where obstacles continue to shift. Additionally, the computation time for a single planning cycle may exceed the horizon of the latest generated control sequences, potentially leading to loss of vehicle control. To address these shortcomings of Algorithm 1, our future works will focus on enhancing robustness through more reliable searching methods and conducting a detailed analysis of general nonlinear vehicle models.

References

- [1] Brian Paden, Michal Čáp, Sze Zheng Yong, Dmitry Yershov, and Emilio Frazzoli. A survey of motion planning and control techniques for self-driving urban vehicles. *IEEE Transactions on Intelligent Vehicles*, 1(1):33–55, 2016.
- [2] Peter E. Hart, Nils J. Nilsson, and Bertram Raphael. A formal basis for the heuristic determination of minimum cost paths. *IEEE Transactions on Systems Science and Cybernetics*, 4(2):100–107, 1968.
- [3] Xiang Liu and Daoxiong Gong. A comparative study of a-star algorithms for search and rescue in perfect maze. In *2011 International Conference on Electric Information and Control Engineering*, pages 24–27, 2011.
- [4] Baichuan Liu, Weikun Zhang, Wuhui Chen, Huawei Huang, and Song Guo. Online computation offloading and traffic routing for uav swarms in edge-cloud computing. *IEEE Transactions on Vehicular Technology*, 69(8):8777–8791, 2020.
- [5] A. Stentz. Optimal and efficient path planning for partially-known environments. In *Proceedings of the 1994 IEEE International Conference on Robotics and Automation*, pages 3310–3317 vol.4, 1994.
- [6] Maxim Likhachev, Geoffrey Gordon, and Sebastian Thrun. Ara*: Anytime a* with provable bounds on sub-optimality. volume 16, 01 2003.
- [7] J.J. Kuffner and S.M. LaValle. Rrt-connect: An efficient approach to single-query path planning. In *Proceedings 2000 ICRA. Millennium Conference. IEEE International Conference on Robotics and Automation. Symposia Proceedings (Cat. No.00CH37065)*, volume 2, pages 995–1001 vol.2, 2000.
- [8] Sertac Karaman, Matthew R. Walter, Alejandro Perez, Emilio Frazzoli, and Seth Teller. Anytime motion planning using the rrt*. In *2011 IEEE International Conference on Robotics and Automation*, pages 1478–1483, 2011.
- [9] Alejandro Perez, Robert Platt, George Konidaris, Leslie Kaelbling, and Tomas Lozano-Perez. Lqr-rrt*: Optimal sampling-based motion planning with automatically derived extension heuristics. In *2012 IEEE International Conference on Robotics and Automation*, pages 2537–2542, 2012.
- [10] Namwook Kim, Sukwon Cha, and Huei Peng. Optimal control of hybrid electric vehicles based on pontryagin’s minimum principle. *IEEE Transactions on Control Systems Technology*, 19(5):1279–1287, 2011.
- [11] Gao Tang, Fanghua Jiang, and Junfeng Li. Fuel-optimal low-thrust trajectory optimization using indirect method and successive convex programming. *IEEE Transactions on Aerospace and Electronic Systems*, 54(4):2053–2066, 2018.
- [12] F. Yegenoglu, A.M. Erkmen, and H.E. Stephanou. Online path planning under uncertainty. In *Proceedings of the 27th IEEE Conference on Decision and Control*, pages 1075–1079 vol.2, 1988.
- [13] Ola Shorinwa, Trevor Halsted, Javier Yu, and Mac Schwager. Distributed optimization methods for multi-robot systems: Part 1—a tutorial [tutorial]. *IEEE Robotics & Automation Magazine*, 31(3):121–138, 2024.
- [14] Jun Ma, Zilong Cheng, Xiaoxue Zhang, Masayoshi Tomizuka, and Tong Heng Lee. Alternating direction method of multipliers for constrained iterative lqr in autonomous driving. *IEEE Transactions on Intelligent Transportation Systems*, 23(12):23031–23042, 2022.
- [15] Behçet Açıkmeşe and Scott R. Ploen. Convex programming approach to powered descent guidance for mars landing. *Journal of Guidance, Control, and Dynamics*, 30(5):1353–1366, 2007.
- [16] Federico Augugliaro, Angela P. Schoellig, and Raffaello D’Andrea. Generation of collision-free trajectories for a quadrocopter fleet: A sequential convex programming approach. In *2012 IEEE/RSJ International Conference on Intelligent Robots and Systems*, pages 1917–1922, 2012.
- [17] Danylo Malyuta, Taylor P. Reynolds, Michael Szmuk, Thomas Lew, Riccardo Bonalli, Marco Pavone, and Behçet Açıkmeşe. Convex optimization for trajectory generation: A tutorial on generating dynamically feasible trajectories reliably and efficiently. *IEEE Control Systems Magazine*, 42(5):40–113, 2022.
- [18] Nicolò Bernardini, Nicola Baresi, and Roberto Armellin. State-dependent trust region for successive convex programming for autonomous spacecraft. *Astrodynamic*, 8(4):553–575, December 2024.
- [19] Riccardo Bonalli, Abhishek Cauligi, Andrew Bylard, and Marco Pavone. Gusto: Guaranteed sequential trajectory optimization via sequential convex programming. In *2019 International Conference on Robotics and Automation (ICRA)*, pages 6741–6747, 2019.
- [20] Patrick Scheffe, Theodor Mario Henneken, Maximilian Kloock, and Bassam Alrifae. Sequential convex programming methods for real-time optimal trajectory planning in autonomous vehicle racing. In *2024 IEEE Intelligent Vehicles Symposium (IV)*, pages 3144–3144, 2024.
- [21] O. Khatib. Real-time obstacle avoidance for manipulators and mobile robots. In *Proceedings. 1985 IEEE International Conference on Robotics and Automation*, volume 2, pages 500–505, 1985.
- [22] Claudio De Medio and Giuseppe Oriolo. Robot obstacle avoidance using vortex fields. In Sabine Stifter and Jadran Lenarčić, editors, *Advances in Robot Kinematics*, pages 227–235, Vienna, 1991. Springer Vienna.

[23] Yan Gao, Dazhi Li, Zhen Sui, and Yantao Tian. Trajectory planning and tracking control of autonomous vehicles based on improved artificial potential field. *IEEE Transactions on Vehicular Technology*, 73(9):12468–12483, 2024.

[24] R. Szczepanski. Safe artificial potential field - novel local path planning algorithm maintaining safe distance from obstacles. *IEEE Robotics and Automation Letters*, 8(8):4823–4830, 2023.

[25] Wang Di, Li Caihong, Guo Na, Song Yong, Gao Tengteng, and Liu Guoming. Local path planning of mobile robot based on artificial potential field. In *2020 39th Chinese Control Conference (CCC)*, pages 3677–3682, 2020.

[26] Rafael Monteiro Jorge Alves Souza, Gabriela Vieira Lima, Aniel Silva Moraes, Luís Cláudio Oliveira-Lopes, Daniel Costa Ramos, and Fernando Lessa Tofoli. Modified artificial potential field for the path planning of aircraft swarms in three-dimensional environments. *Sensors*, 22(4), 2022.

[27] Claudio De Medio and Giuseppe Oriolo. Robot obstacle avoidance using vortex fields. In Sabine Stifter and Jadran Lenarčič, editors, *Advances in Robot Kinematics*, pages 227–235, Vienna, 1991. Springer Vienna.

[28] D. Fox, W. Burgard, and S. Thrun. The dynamic window approach to collision avoidance. *IEEE Robotics & Automation Magazine*, 4(1):23–33, 1997.

[29] O.L Mangasarian and S Fromovitz. The fritz john necessary optimality conditions in the presence of equality and inequality constraints. *Journal of Mathematical Analysis and Applications*, 17(1):37–47, 1967.

[30] Inc. CVX Research. CVX: Matlab software for disciplined convex programming, version 2.0. <https://cvxr.com/cvx>, August 2012.

[31] M. Grant and S. Boyd. Graph implementations for nonsmooth convex programs. In V. Blondel, S. Boyd, and H. Kimura, editors, *Recent Advances in Learning and Control*, Lecture Notes in Control and Information Sciences, pages 95–110. Springer-Verlag Limited, 2008. http://stanford.edu/~boyd/graph_dcp.html.

A Proof of Theorem 2

We consider the Lagrangian $\mathcal{L}_{m'+n}(z_0; \cdot)$. If $\{z_1^*, z_2^*, \dots, z_{m'+n+1}^*; u_1^*, \dots, u_{m'+n}^*\}$ with the corresponding Lagrange multipliers locally solves $\mathcal{P}_1(z_0; m' + n)$, we can immediately list the following KKT conditions:

$$\begin{aligned} \frac{\partial \mathcal{L}_{m'+n}(z_0; \cdot)}{\partial z_i^*} &= \frac{\partial}{\partial z_i^*} \sum_{j=1}^{n_{\text{obs}}} \zeta_{ij}^* \left(r_j^2 - \|z_i^*[1:2] - p_j\|^2 \right) \\ &\quad - \frac{\partial f^\top}{\partial z_i^*} \cdot v_i^* + v_{i-1}^* + 2s_i^* Q_1 z_i^* \\ &= \mathbf{0}, \end{aligned} \quad (\text{A.1a})$$

$$\frac{\partial \mathcal{L}_{m'+n}(z_0; \cdot)}{\partial u_i^*} = -\frac{\partial f^\top}{\partial u_i^*} \cdot v_i^* + 2q_i^* Q_2 u_i^* = \mathbf{0}, \quad (\text{A.1b})$$

$$v_i^* (z_{i+1}^* - f(z_i^*, u_i^*)) = \mathbf{0}, \quad (\text{A.1c})$$

$$\zeta_{ij}^* \left(r_j^2 - \|z_i^*[1:2] - p_j\|^2 \right) = \mathbf{0}, \quad (\text{A.1d})$$

$$s_i^* G_1(z_i^*) = 0, \quad (\text{A.1e})$$

$$q_i^* G_2(u_i^*) = 0, \quad (\text{A.1f})$$

$$v_i^*, \zeta_{ij}^*, q_i^*, s_i^* \geq 0, \quad (\text{A.1g})$$

and for $i = m' + n + 1$, there exist

$$\begin{aligned} \frac{\partial \mathcal{L}_{m'+n}(z_0; \cdot)}{\partial z_i^*} &= \frac{\partial}{\partial z_i^*} \sum_{j=1}^{n_{\text{obs}}} \zeta_{ij}^* \left(r_j^2 - \|z_i^*[1:2] - p_j\|^2 \right) \\ &\quad - \frac{\partial f^\top}{\partial z_i^*} v_i^* + v_{m'+n}^* + 2s_i^* Q_1 z_i^* \\ &= \mathbf{0}. \end{aligned} \quad (\text{A.1h})$$

For (A.1a), the range of i is $2 \leq i \leq m' + n + 1$, for (A.1b), (A.1c), (A.1e), (A.1f), the range of i is $1 \leq i \leq m' + n$, while for (A.1d), the index range is $1 \leq i \leq m' + n + 1$. Similarly, the optimizer of $\mathcal{P}_1(z_0; m)$, namely $\{z_1^1, z_2^1, \dots, z_{m+1}^1; u_1^1, \dots, u_m^1\}$, must satisfy

$$\begin{aligned} \frac{\partial \mathcal{L}_m(z_0; \cdot)}{\partial z_i^1} &= \frac{\partial}{\partial z_i^1} \sum_{j=1}^{n_{\text{obs}}} \zeta_{ij}^1 \left(r_j^2 - \|z_i^1[1:2] - p_j\|^2 \right) \\ &\quad - \frac{\partial f^\top}{\partial z_i^1} v_i^1 + v_{i-1}^1 + 2s_i^1 Q_1 z_i^1 \\ &= \mathbf{0}, \end{aligned} \quad (\text{A.2a})$$

$$\frac{\partial \mathcal{L}_m(z_0; \cdot)}{\partial u_i^1} = -\frac{\partial f^\top}{\partial u_i^1} v_i^1 + 2q_i^1 Q_2 u_i^1 = \mathbf{0}, \quad (\text{A.2b})$$

$$v_i^1 (z_{i+1}^1 - f(z_i^1, u_i^1)) = \mathbf{0}, \quad (\text{A.2c})$$

$$\zeta_{ij}^1 \left(r_j^2 - \|z_i^1[1:2] - p_j\|^2 \right) = \mathbf{0}, \quad (\text{A.2d})$$

$$s_i^1 G_1(z_i^1) = 0, \quad (\text{A.2e})$$

$$q_i^1 G_2(u_i^1) = 0, \quad (\text{A.2f})$$

$$v_i^1, \zeta_{ij}^1, q_i^1, s_i^1 \geq 0 \quad (\text{A.2g})$$

with some multipliers $v_i^1, \zeta_{ij}^1, q_i^1, s_i^1$. In (A.2a)-(A.2g), the range of i is $1 \leq i \leq m'$ for (A.2b), (A.2c), (A.2f), $1 \leq m'+1$ for (A.2d), (A.2e) while $2 \leq i \leq m'+1$ for (A.2a). For $\{z_1^2, z_2^2, \dots, z_{n+1}^2; u_1^2, \dots, u_n^2\}$ with the corresponding multipliers $\{v_i^2, \zeta_{ij}^2, q_i^2, s_i^2\}$, we have

$$\begin{aligned} \frac{\partial \mathcal{L}_n(z_1^2; \cdot)}{\partial z_i^2} &= \frac{\partial}{\partial z_i^2} \sum_{j=1}^{n_{\text{obs}}} \zeta_{ij}^2 \left(r_j^2 - \|z_i^2[1:2] - p_j\|^2 \right) \\ &\quad - \frac{\partial f^\top}{\partial z_i^2} v_i^2 + v_{i-1}^2 + 2s_i^2 Q_1 z_i^2 \\ &= \mathbf{0}, \end{aligned} \quad (\text{A.3a})$$

$$\frac{\partial \mathcal{L}_n(z_1^2; \cdot)}{\partial u_i^2} = -\frac{\partial f^\top}{\partial u_i^2} v_i^2 + 2q_i^2 Q_2 u_i^2 = \mathbf{0}, \quad (\text{A.3b})$$

$$v_i^2 (z_{i+1}^2 - f(z_i^2, u_i^2)) = \mathbf{0}, \quad (\text{A.3c})$$

$$\zeta_{ij}^2 \left(r_j^2 - \|z_i^2[1:2] - p_j\|^2 \right) = \mathbf{0}, \quad (\text{A.3d})$$

$$s_i^2 G_1(z_i^2) = 0, \quad (\text{A.3e})$$

$$u_i^2 G_2(u_i^2) = 0, \quad (\text{A.3f})$$

$$v_i^2, \zeta_{ij}^2, q_i^2, s_i^2 \geq 0 \quad (\text{A.3g})$$

for appropriate indexes i, j and

$$\frac{\partial \mathcal{L}_n(z_n^2; \cdot)}{\partial z_{n+1}^2} = \frac{\partial}{\partial z_{n+1}^2} \sum_{j=1}^{n_{\text{obs}}} \zeta_{n+1,j}^2 \left(r_j^2 - \|z_n^2[1:2] - p_j\|^2 \right)$$

$$-\frac{\partial f}{\partial z_i^2}^\top v_{n+1}^2 + v_n^2 + 2s_{n+1}^2 Q_1 z_{n+1}^2 = \mathbf{0}. \quad (\text{A.3h})$$

Now, we take $z_1 = z_1^1$, $z_2 = z_2^1$, \dots , $z_{m'+1} = z_{m'+1}^1$, $z_{m'+2} = z_2^2$, \dots , $z_{m'+n+1} = z_{n+1}^2$ and $u_1 = u_1^1, \dots, u_{m'} = u_{m'}^1, u_{m'+1} = u_2^1, \dots, u_{m'+n} = u_n^2$, and define

$$\begin{aligned} \mathbf{Z} &:= \{z_1, z_2, \dots, z_{m'+n+1}\}, \\ \mathbf{U} &:= \{u_1, u_2, \dots, u_{m'+n}\}, \\ \boldsymbol{\zeta} &:= \{\zeta_{1j}^1, \zeta_{2j}^1, \dots, \zeta_{m'+1,j}^1, \zeta_{2j}^2, \dots, \zeta_{n+1,j}^2\}_{j=1}^{n_{obs}}, \\ \mathbf{v} &:= \{v_1^1, \dots, v_{m'+1}^1, v_2^2, \dots, v_{n+1}^2\}, \\ \mathbf{q} &:= \{q_1^1, \dots, q_{m'+1}^1, q_2^2, \dots, q_{n+1}^2\}, \\ \mathbf{s} &:= \{s_1^1, \dots, s_{m'+1}^1, s_2^2, \dots, s_{n+1}^2\}. \end{aligned}$$

We then show that $\{\mathbf{Z}, \mathbf{U}, \boldsymbol{\zeta}, \mathbf{v}, \mathbf{q}, \mathbf{s}\}$ reaches a KKT point of $\mathcal{L}_{m'+n}(z_0, \cdot)$. In fact, we only need to show $\frac{\partial \mathcal{L}_{m'+n}(z_0, \cdot)}{\partial z_{m'+2}} = \mathbf{0}$, namely, to prove

$$\begin{aligned} &\frac{\partial}{\partial z_{m'+1}} \sum_{j=1}^{n_{obs}} \zeta_{m'+2,j} (r_j^2 - \|z_{m'+2}[1:2] - p_j\|^2) \\ &- \frac{\partial f}{\partial z_{m'+2}}^\top v_{m'+2} + v_{m'+1} = \mathbf{0} \end{aligned} \quad (\text{A.4})$$

as (A.2a)-(A.2g) and (A.3a)-(A.3h) profile all other KKT conditions of $\mathcal{L}_{m'+n}(z_0, \cdot)$ for the given variables $\{\mathbf{Z}, \mathbf{U}, \boldsymbol{\zeta}, \mathbf{v}, \mathbf{q}, \mathbf{s}\}$. If $u_1^2 Q_2 u_1^2 < 1$, then $q_{m'+1} = q_1^2 = 0$. As a result, combining with (A.3b), we can obtain

$$-\frac{\partial f}{\partial u_1^2}^\top v_1^2 + 2q_1^2 Q_2 u_1^2 = -\frac{\partial f}{\partial u_1^2}^\top v_1^2 + \mathbf{0} = \mathbf{0},$$

which apparently indicates $v_1^2 = \mathbf{0}$ since $\frac{\partial f}{\partial u_1^2}$ is of full column rank. Similarly, we have $v_{m'+1}^1 = \mathbf{0}$. That means

$$\begin{aligned} &\frac{\partial}{\partial z_2^2} \sum_{j=1}^{n_{obs}} \zeta_{2,j}^2 (r_j^2 - \|z_2^2[1:2] - p_j\|^2) \\ &- \frac{\partial f}{\partial z_2^2}^\top v_2^2 + v_{m'+1}^1 = \mathbf{0} \end{aligned} \quad (\text{A.5})$$

as we substitute v_1^2 by $v_{m'+1}^1$. By further substituting $v_2^2 = v_{m'+2}$, $v_{m'+1}^1 = v_{m'+1}$, $z_2^2 = z_{m'+2}$, $\zeta_{2,j}^2 = \zeta_{m'+2,j}$ into (A.5), we get (A.4). This completes the proof. \square

B Proof of Theorem 4

For simplicity, the indicator of iteration order are omitted, e.g. $z^{(K)}$ is abbreviate as z . Take $\rho = 0$. Recall that the Lagrange function of $\mathcal{P}_1(z_0; N, \cdot)$ can be formulated as $\mathcal{L}_N(z_0; z, u, v, \zeta, s, q)$, with the same form of the template (31). For the optimizer of \mathcal{L}_N with the corresponding multipliers, the KKT conditions are obtained as

$$\begin{cases} Az_i^* + Bu_i^* - z_{i+1}^* = \mathbf{0}, \\ s_i^* G_1(z_i^*) = \mathbf{0}, \\ q_i^* G_2(u_i^*) = \mathbf{0}, \\ \zeta_{ij}^* (r_j^2 - \|z_i^*[1:2] - p_j\|^2) = \mathbf{0}, \\ s_i^* \geq 0, q_i^* \geq 0, \zeta_{ij}^* \geq 0, \\ z_1^* = z_0, \end{cases}$$

and

$$\{z_i^*, u_i^*\} = \arg \min_{z_i, u_i} \mathcal{L}_N \quad (\text{B.1})$$

with proper indexes i under Assumption 5. Our goal is to show the computed state-control series $\{z_1, \dots, z_{N+1}; u_1, \dots, u_N\}$ by the optimizer of $\mathcal{P}_s(z_0; N, \cdot)$ satisfies the above KKT conditions. Take

$$\mathcal{L}'_N = \mathcal{L}_N - \sum_{i=1}^{N+1} \sum_{j=1}^{n_{obs}} \zeta_{ij} (r_j^2 - \|z_i[1:2] - p_j\|^2).$$

Then, for such $\mathcal{P}_s(\cdot)$, the corresponding Lagrange function can be formed as

$$\begin{aligned} \mathcal{L}_s(z_0; z, u, v, \eta, \sigma, \xi, s, q) &= \mathcal{L}'_N \\ &+ \sum_{i=1}^{N+1} (\eta_i - \sigma_i) \lambda_{f,i} - \eta_i + \sum_{i=1}^{N+1} \xi_i (\lambda_{d,i} - k_i \lambda_{f,i}), \end{aligned} \quad (\text{B.2})$$

where η_i, σ_i, ξ_i are Lagrange multipliers. If $\lambda_{\min,i} = 0$ holds for arbitrary i , then the nominal trajectory itself is feasible, which is also a minimizer of \mathcal{L}_N . Otherwise, if a relative interior solution is obtained, we have $\zeta_{ij}^* = \eta_i^* = \sigma_i^* = \xi_i^* = 0$ for all i by complement slackness condition. Actually, now we can obtain that $\mathcal{L}_s \equiv \mathcal{L}_N$. The first order optimality conditions of the strict problem are

$$\begin{cases} \frac{\partial \mathcal{L}_s}{\partial \lambda_{f,i}^*} = 0, \\ \frac{\partial \mathcal{L}_s}{\partial \lambda_{d,i}^*} = 0 \end{cases} \quad (\text{B.3})$$

or

$$\{\lambda_{f,i}^*, \lambda_{d,i}^*\} = \arg \min_{\lambda_{f,i}, \lambda_{d,i}} \mathcal{L}_s. \quad (\text{B.4})$$

In $\mathcal{P}_s(\cdot)$, it is worth noting that one pair of $\{\lambda_{f,i}, \lambda_{d,i}\}$ determines $\{z_i\}_{i=1}^{N+1}$ uniquely. With Assumption 4, we further obtain that a given $\{\lambda_{f,i}, \lambda_{d,i}\}$ determines a unique $\{z_1, \dots, z_{N+1}; u_1, \dots, u_N\}$. In other words, (B.4) is a sufficient condition of (B.1). Thereby, we complete the proof. \square

C Proof of Theorem 5

It is easy to obtain two properties of Φ_Θ : (i) since the minimizer of Φ_Θ is a singleton (according to the precondition), we have $\Phi_\Theta(\Theta_{opt}) = \Phi_\Theta(\Theta_{opt}^+) = 0$; (ii) for $s_1 \geq s_2 \geq \Theta_{opt}$, we have

$$\begin{aligned} \Phi_\Theta(s_1) &= \text{diam}(\text{Lev}(\Theta, s_1)) \\ &\geq \text{diam}(\text{Lev}(\Theta, s_2)) = \Phi_\Theta(s_2) \geq 0. \end{aligned}$$

Suppose Φ is not upper semi-continuous at $\tilde{s} > \Theta_{opt}$. Then, leveraging the monotonic non-decrease property of Φ_Θ , for any given $\delta > 0$, there exists an $\epsilon > 0$ with

$$\Phi_\Theta(\tilde{s} + \delta) - \Phi_\Theta(\tilde{s}) \geq \epsilon. \quad (\text{C.1})$$

Suppose $\mathbf{x}(\tilde{s}), \mathbf{y}(\tilde{s})$ are one pair of the cluster points of $\text{Lev}(\Theta, \tilde{s})$ where their distance reaches $\text{diam}(\text{Lev}(\Theta, \tilde{s}))$. Then, with (C.1) we can derive

$$\begin{aligned} \Phi_\Theta(\tilde{s} + \delta) - \Phi_\Theta(\tilde{s}) &= \|\mathbf{x}(\tilde{s} + \delta) - \mathbf{y}(\tilde{s} + \delta)\| \\ &\quad - \|\mathbf{x}(\tilde{s}) - \mathbf{y}(\tilde{s})\| \end{aligned}$$

$$\begin{aligned} &\leq \|\mathbf{x}(\tilde{s} + \delta) - \mathbf{x}(\tilde{s})\| \\ &\quad + \|\mathbf{y}(\tilde{s} + \delta) - \mathbf{y}(\tilde{s})\|. \end{aligned} \quad (\text{C.2})$$

Thus, we have

$$\|\mathbf{x}(\tilde{s} + \delta) - \mathbf{x}(\tilde{s})\| + \|\mathbf{y}(\tilde{s} + \delta) - \mathbf{y}(\tilde{s})\| \geq \epsilon. \quad (\text{C.3})$$

Since (C.3) holds for arbitrary $\{\mathbf{x}(\tilde{s} + \delta), \mathbf{y}(\tilde{s} + \delta)\} \subset \text{cl}(\text{diam}(\text{Lev}(\Theta, \tilde{s} + \delta)))$ with $\|\mathbf{x}(\tilde{s} + \delta) - \mathbf{y}(\tilde{s} + \delta)\| = \Phi_\Theta(\tilde{s} + \delta)$, we can further obtain

$$\begin{aligned} \epsilon &\leq \min_{\mathbf{x}(\tilde{s} + \delta), \mathbf{y}(\tilde{s} + \delta)} \{\|\mathbf{x}(\tilde{s} + \delta) - \mathbf{x}(\tilde{s})\| \\ &\quad + \|\mathbf{y}(\tilde{s} + \delta) - \mathbf{y}(\tilde{s})\|\}. \end{aligned} \quad (\text{C.4})$$

Utilize the fact that all the strict **sublevel** sets are open, we can derive $\mathbf{x}(\tilde{s}), \mathbf{y}(\tilde{s})$ lie on the boundary of $\text{cl}(\text{Lev}(\Theta, \tilde{s}))$ with $\Theta(\mathbf{x}(\tilde{s})) = \Theta(\mathbf{y}(\tilde{s})) = \tilde{s}$. Then, by choosing a non-increasing series $\{\delta_n\}$ which converges to 0, we have

$$\begin{aligned} &\left(\lim_{\delta \rightarrow 0^+} \text{Lev}(\Theta, \tilde{s} + \delta) \right) \setminus \text{Lev}(\Theta, \tilde{s}) \\ &= \left(\lim_{n \rightarrow \infty} \bigcap_{i=1}^n \text{Lev}(\Theta, \tilde{s} + \delta_i) \right) \setminus \text{Lev}(\Theta, \tilde{s}) \\ &= \overline{\text{Lev}}(\Theta, \tilde{s}) \setminus \text{Lev}(\Theta, \tilde{s}) \\ &= \{\mathbf{x} \mid \Theta(\mathbf{x}) = \tilde{s}\}. \end{aligned} \quad (\text{C.5})$$

By (C.4), at least one inequality of

$$\begin{cases} \|\mathbf{x}(\tilde{s} + \delta) - \mathbf{x}(\tilde{s})\| \geq \epsilon/2, \\ \|\mathbf{y}(\tilde{s} + \delta) - \mathbf{y}(\tilde{s})\| \geq \epsilon/2 \end{cases}$$

holds as $\delta \rightarrow 0^+$, which indicates that $\mathbf{x}(\tilde{s} + \delta)$ or $\mathbf{y}(\tilde{s} + \delta)$ is out of $\text{cl}(\text{Lev}(\Theta, \tilde{s}))$ (Note that the fact holds since once $\mathbf{x}(\tilde{s} + \delta), \mathbf{y}(\tilde{s} + \delta) \in \text{cl}(\text{Lev}(\Theta, \tilde{s}))$, (C.1) and (C.4) cannot be satisfied simultaneously). Hence, suppose $\|\mathbf{x}(\tilde{s} + \delta) - \mathbf{x}(\tilde{s})\| \geq \epsilon/2$ as $\delta \rightarrow 0^+$, we can found a \mathbf{x}^\dagger with $\mathbf{x}^\dagger \notin \text{cl}(\text{Lev}(\Theta, \tilde{s}))$, $\mathbf{x}^\dagger \in (\text{Lev}(\Theta, \tilde{s}) \cup \{\mathbf{x} \mid \Theta(\mathbf{x}) = \tilde{s}\}) \setminus \text{Lev}(\Theta, \tilde{s})$. Note

$$\overline{\text{Lev}}(\Theta, \tilde{s}) = \left(\lim_{n \rightarrow \infty} \bigcap_{i=1}^n \text{Lev}(\Theta, \tilde{s} + \delta_i) \right),$$

which preserves the convexity of $\overline{\text{Lev}}(\Theta, \tilde{s})$. Moreover, we have

$$\begin{aligned} &\text{conv}(\text{Lev}(\Theta, \tilde{s}), \mathbf{x}^\dagger) \setminus \text{Lev}(\Theta, \tilde{s}) \\ &\subset \overline{\text{Lev}}(\Theta, \tilde{s}) \setminus \text{Lev}(\Theta, \tilde{s}) \\ &= \{\mathbf{x} : \Theta(\mathbf{x}) = \tilde{s}\}. \end{aligned} \quad (\text{C.6})$$

By (C.6), there exists some interior points in $\{\mathbf{x} \mid \Theta(\mathbf{x}) = \tilde{s}\}$. Take $\mathbf{x}^* \in \text{int}\{\mathbf{x} \mid \Theta(\mathbf{x}) = \tilde{s}\}$, then there exists $\mathcal{B}(\mathbf{x}^*, r)$ with $\Theta(\mathbf{x}) \equiv \tilde{s}$ for any $\mathbf{x} \in \mathcal{B}(\mathbf{x}^*, r)$, which indicates $\mathbf{0} \in \partial\Theta(\mathbf{x}^*)$. By Fermat condition and the convexity of Θ , \mathbf{x}^* is an optimizer of Θ . However, with $\Theta(\mathbf{x}^*) = \tilde{s} > \Theta_{opt}$, the optimality of \mathbf{x}^* contradicts to the convexity. Hence, Φ_f cannot be discontinuous at $\tilde{s} \in (\Theta_{opt}, \infty)$. Combining with (i), we can further derive that $\Phi_\Theta(s)$ is upper semi-continuous for $s \in [\Theta_{opt}, \infty)$. This completes the proof. \square

In the proof, if Θ is defined in \mathbb{R}^{ℓ_Θ} , then $\Theta : \mathbb{E} \rightarrow \mathbb{R}$ can also written as Θ' :

$$\Theta'(\mathbf{x}) = \begin{cases} \Theta(\mathbf{x}) + I_{\mathbb{E}}(\mathbf{x}), & \mathbf{x} \in \mathbb{E}, \\ I_{\mathbb{E}}(\mathbf{x}), & \mathbf{x} \notin \mathbb{E}, \end{cases}$$

where $I_{\mathbb{E}}$ is the indicator function defined by

$$I_{\mathbb{E}}(\mathbf{x}) := \begin{cases} 0, & \mathbf{x} \in \mathbb{E}, \\ \infty, & \mathbf{x} \notin \mathbb{E}. \end{cases}$$

D Proof of Theorem 6

We still use the notation $\Phi_\Theta(s)$ to represent $\text{diam}(\text{Lev}(\Theta, s))$. Suppose there are two non-empty strict **sublevel** sets $L_1 = \text{Lev}(\Theta, s_1)$ and $L_2 = \text{Lev}(\Theta, s_2)$, where $\Phi_\Theta(s_1) = D_1$, $\Phi_\Theta(s_2) = D_2$ and $D_2 > D_1 \geq \Phi_\Theta(\Theta_{opt}^+)$. Take $\mathbf{x}^*(D_1) \in \text{cl}(L_1)$, $\mathbf{x}^*(D_2) \in \text{cl}(L_2)$ with $\mathbf{y}^*(L_1), \mathbf{y}^*(L_2)$ being their corresponding projection on X^* . Then, we have

$$\begin{aligned} 0 &\leq \|\mathbf{x}^*(L_2) - \mathbf{y}^*(L_2)\| - \|\mathbf{x}^*(L_1) - \mathbf{y}^*(L_1)\| \\ &\leq \|\mathbf{x}^*(L_2) - \mathbf{x}^*(L_1)\| + \|\mathbf{y}^*(L_2) - \mathbf{y}^*(L_1)\| \\ &\leq 2\|\mathbf{x}^*(L_2) - \mathbf{x}^*(L_1)\|. \end{aligned} \quad (\text{D.1})$$

By the boundness of X^* , $\Phi_\Theta(\Theta_{opt}^+) < \infty$ holds. We first prove (D.1) converges to 0 as $D_2 - D_1 \rightarrow 0$. Suppose there exists $\epsilon > 0$ making $\|\mathbf{x}^*(L_2) - \mathbf{y}^*(L_2)\| - \|\mathbf{x}^*(L_1) - \mathbf{y}^*(L_1)\| \geq \epsilon$ for any $D_2 > D_1 > \text{diam}(X^*)$, then utilizing (D.1) we can obtain $\min\{\|\mathbf{x}^*(L_2) - \mathbf{x}^*(L_1)\|\} > \frac{\epsilon}{2}$. By the continuity of Θ , we can further obtain

$$\min\{\|\mathbf{x}^*(L_1) - \mathbf{x}^*(L_1)\|\} = 0 > \frac{\epsilon}{2}$$

as $D_2 \rightarrow D_1$, which contradicts to $\epsilon > 0$. Therefore,

$$\max_{\mathbf{x} \in \text{cl}(\text{Lev}(\Theta, s))} \|\mathbf{x} - \text{Proj}_{X^*}(\mathbf{x})\| \quad (\text{D.2})$$

is an upper semi-continuous function of D for $D \in [\Phi_\Theta(\Theta_{opt}^+), \Phi_\Theta(+\infty))$. Moreover, by utilizing (D.2) we can obtain

$$\varphi(\Theta_{opt}) = 0 = \varphi(\Theta_{opt}^+). \quad (\text{D.3})$$

This completes the proof. \square